

Resubmitted for the CCCP Special Issue, February 18, 2011

## The Chandra Carina Complex Project View of Trumpler 16

Scott J. Wolk<sup>1</sup>, Patrick S. Broos<sup>2</sup>, Konstantin V. Getman<sup>2</sup>, Eric D. Feigelson<sup>2</sup>, Thomas Preibisch<sup>3</sup>, Leisa K. Townsley<sup>2</sup>, Junfeng Wang<sup>1</sup>, Keivan G. Stassun<sup>4,5</sup>, Robert R. King<sup>6</sup>, Mark J. McCaughrean<sup>6,7</sup>, Anthony F. J. Moffat<sup>8</sup> and Hans Zinnecker<sup>9</sup>

### ABSTRACT

Trumpler 16 is a well-known rich star cluster containing the eruptive supergiant  $\eta$  Carinae and located in the Carina star-forming complex. In the context of the *Chandra Carina Complex Project*, we study Trumpler 16 using new and archival X-ray data. A revised X-ray source list of the Trumpler 16 region contains 1232 X-ray sources including 1187 likely Carina members. These are matched to 1047 near-infrared counterparts detected by the HAWK-I instrument at the VLT allowing for better selection of cluster members. The cluster is irregular in shape. Although it is roughly circular, there is a high degree of sub-clustering, no noticeable central concentration and an extension to the southeast. The high-mass stars show neither evidence of mass segregation nor evidence of strong differential extinction. The derived power-law slope of the X-ray luminosity function for Trumpler 16 reveals a much steeper function than the Orion Nebula Cluster implying different ratio of solar- to higher-mass stars. We estimate the total Trumpler 16 pre-main sequence population to be  $> 6500$  Class II and Class III X-ray sources. An overall K-excess disk frequency of  $\sim 8.9\%$  is derived using the X-ray selected sample, although there is some variation among the sub-clusters, especially in the Southeastern extension. X-ray emission is detected from 29 high-mass stars with spectral types between B2 and O3.

---

<sup>1</sup>Harvard-Smithsonian Center for Astrophysics, 60 Garden Street, Cambridge, MA 02138, USA

<sup>2</sup>Department of Astronomy & Astrophysics, The Pennsylvania State University, 525 Davey Lab, University Park, PA 16802, USA

<sup>3</sup>Universitäts-Sternwarte, Ludwig-Maximilians-Universität, Scheinerstr. 1, 81679 München, Germany

<sup>4</sup>Department of Physics & Astronomy, Vanderbilt University, Nashville, TN 37235, USA

<sup>5</sup>Department of Physics, Fisk University, 1000 17th Ave. N., Nashville, TN 37208, USA

<sup>6</sup>Astrophysics Group, College of Engineering, Mathematics, and Physical Sciences, University of Exeter, Exeter EX4 4QL, UK

<sup>7</sup>European Space Agency, Research & Scientific Support Department, ESTEC, Postbus 299, 2200 AG Noordwijk, The Netherlands

<sup>8</sup>Département de Physique, Université de Montréal, Succursale Centre-Ville, Montréal, QC, H3C 3J7, Canada

<sup>9</sup>Deutsches SOFIA Institute, Univ. of Stuttgart, Germany and NASA-Ames Research Center, USA

*Subject headings:* ISM: individual (Great Nebula in Carina) - open clusters and associations: individual (Trumpler 16) - stars: pre-main sequence - X-Rays: stars X-ray – Facilities: Chandra, VLT

## 1. Introduction

Trumpler 16 lies at the heart of the Carina Nebula region. It includes three main sequence O3 stars, the Wolf-Rayet star WR 25 and  $\eta$  Carinae.  $\eta$  Carinae first became notable when it brightened significantly in the 1840s (Herschel 1847). During that event an estimated  $\gtrsim 10 M_{\odot}$  of material and nearly  $10^{50}$  ergs of kinetic energy were injected into the host cluster (Smith et al. 2003). Prior to the event,  $\eta$  Carinae most likely dominated the energy budget of the cluster. Since this event however,  $\eta$  Carinae has been essentially cut off from the cluster due to the vast opaque shell surrounding it. This shell is surrounded by the Homunculus nebula (Gaviola 1950) which itself is a subset of a massive HII region spanning several square degrees. The 2.3 kpc distance to the cluster comes primarily from the expansion parallax of the Homunculus nebula around  $\eta$  Carinae (Smith 2006, Davidson and Humphreys 1997).

The stellar content and star formation history of Trumpler 16 has been studied in the optical band. Early studies concentrated on the massive stars. Walborn (1971, 1973) identified 6 Henry Draper stars within Trumpler 16 and the neighboring cluster, Trumpler 14, which were more massive than any star known at that time, leading to the introduction of the O3 classification. This implied both a very high mass and young age for these cluster. Levato & Malaroda (1982) and Morrell et al. (1988) identified many more O stars in these clusters spectroscopically. Feinstein (1982) performed deep photomultiplier-based observations of about 70 cluster members as faint as  $V \approx 14$ . An early CCD-based photometric study by Massey & Johnson (1993) reached about  $1 M_{\odot}$ . This was followed by Degioia–Eastwood et al. (2001) who presented optical photometry for over 560 stars in Trumpler 16. They found clear evidence of pre-main sequence stars in the region and argued for a mass-dependent spread in ages with intermediate mass star forming continuously over the past 10 million years and high mass stars forming within the last 3 million years.

An inventory of Trumpler 16 includes 42 O stars with the total radiative luminosity equal to  $\log(L/L_{\odot}) = 7.24$ , a total mass loss equal to  $1.08 \times 10^{-3} M_{\odot}$  per year and mechanical luminosity of  $6.7 \times 10^4 L_{\odot}$  in the wind (Smith 2006). The region includes 12 small Bok globules including the “Keyhole Nebula”, the “Kangaroo Nebula”, and “The Finger” (Smith & Brooks 2008). Whether or not these are sites of ongoing star formation remains an open question. The region is dominated by ionized gas emission. The strong 1.2 mm continuum is dominated by free–free emission, not cool dust (Brooks et al. 2005).

In the X-ray regime, this is a very well studied cluster. Albacete–Colombo et al. (2003) observed this region with *XMM – Newton* for 35 ks and detected 80 of the brightest sources, but this observation was badly limited by source confusion. Evans et al. (2003) used 9.3 ks of

early Chandra data to study the hardness ratios of the hot stars in Trumpler 16. The luminosity limit of that Chandra observation was about  $7 \times 10^{31} \text{ ergs s}^{-1}$ , typical of single O and early B stars. Albacete–Colombo re-observed the cluster with Chandra for 90 ks. They found 1035 sources and matched 660 to 2MASS counterparts (Albacete–Colombo et al. 2008; AC08). About 15% of the X-ray sources with near IR counterparts were found to have infrared excesses indicative of an optically thick disk in the  $K_S$  band. While the AC08 study covered a square  $17'$  by  $17'$  ACIS-I field which included part of Trumpler 14, the analysis presented by Feigelson et al. (2011; hereafter Paper I) shows that Trumpler 16 occupies only a portion of the ACIS-I field studied by AC08. In the north, Trumpler 16 is roughly circular about  $11.6'$  across while towards the southeast it has an extension about  $10'$  by  $6'$  (Figure 1). The structure, in part, is caused by an absorption lane that crosses the middle of the field. The highly structured nature of Trumpler 16 is qualitatively different from Trumpler 14 and Trumpler 15 which have a single central concentration (Ascenso et al. 2007, Wang et al. 2011).

The Trumpler 16 region was not re-observed as part of the *Chandra Carina Complex Project* (CCCP; Townsley et al. 2011a); instead previous observations were re-analyzed following the prescriptions described in Broos et al. (2010 and 2011). The purpose of this paper therefore, is not a full discussion of the data, which are presented by AC08, but instead to present the findings in the context of the full X-ray analysis of the Carina complex. We also invoke the new HAWK-I infrared observations (Preibisch et al. 2011) for improved near-infrared counterpart information. For the purpose of this paper, we define Trumpler 16 following the clustering analysis presented by Paper I, in which Trumpler 16 is divided into seven sub clusters and a surrounding matrix of stars.

In the next section, we will review the results of AC08 and compare those results with the re-analysis of the X-ray data using new techniques presented by Broos et al. (2010, 2011). We then evaluate the global extinction due to dust, absorption due to gas, and luminosity properties of the cluster. Next, we study the spatial distribution of the stars concentrating on the several sub-clusters to examine whether the sub-clusters are real physical phenomena. This paper will put little emphasis on high-mass stars except as they pertain exclusively to Trumpler 16, as these stars are discussed elsewhere (Nazé et al. 2011, Gagné et al. 2011). The A0-B3 stars in Tr 16 are examined in detailed by Evans et al. (2011), candidate new OB stars are identified by Povich et al. (2011), and Townsley et al. (2011b) discuss the diffuse emission in the region.

## 2. The Observations and Data Reduction

The bulk of the X-ray data discussed here were taken prior to the CCCP, as part of a guaranteed time program (2006 August 31, PI S. Murray, 88.4 ks, ObsID 6402). A comprehensive analysis of those data was provided by AC08, including discussion of sources in the Trumpler 14 region (to the north of Trumpler 16) and detailed analysis of individual sources that are X-ray bright. In this study we limit our attention to the Trumpler 16 cluster, and we supplement the AC08 data with additional observations that partially overlap Tr 16 (ObsIDs 9482, 9483, 9488, 6578, and 4495),

which are described and mapped by Townsley et al. (2011a; [Table 1]).

We define Trumpler 16 as the region within the lowest contour of the kernel smoothed star surface density distribution shown in Paper I. This is identified by a continuous contour of density to the South and East and terminates in a narrow region separating Trumpler 14 from Trumpler 16 in the Northwest (Figure 1). Trumpler 16 includes the matrix of stars surrounding the 7 sub-clusters identified in Paper I. About 1/8 of the field of view of ObsID 6402 covers Trumpler 14 and about one-third of the area of ObsID 6402 lay outside of either cluster. Lower-density portions of Trumpler 16 to the South and East (which we will refer to as the Trumpler 16 Southeastern extension) were not included in the ObsID 6402 field of view. This includes the CCCP-cluster 14 (Paper I) which has been previously identified by Sanchawala et al. (2007a,b). This region has been covered by other observations as part of the CCCP program and so is included in the analysis presented here.

The 2MASS Survey, which has a completeness limit near the galactic plane of  $K_s \sim 13.3$  (Skrutskie et al. 2006), was the only nearIR (NIR) data available to AC08. Deep NIR observations obtained using the HAWK-I camera at the ESO VLT have recently become available and are used in this study to extend the NIR catalog to a completeness limit of  $K_s \sim 19$  mag and an ultimate detection limit of  $K_s \sim 21$  (Preibisch et al. 2011).

The data reduction, source detection, and source extraction procedures applied to all the CCCP data are described by Broos et al. (2011a). We adopt the statistical classification of sources as likely Carina members, likely contaminants, or “unclassified objects” presented by Broos et al. (2011b), understanding that the individual classifications are not guaranteed to be correct. Column densities and absorption-corrected X-ray luminosities for individual stars were estimated using the photometric techniques of the XPHOT package (Getman et al. 2010).

Briefly, the CCCP source detection strategy was to nominate a liberal catalog of candidate point sources using multiple source finding algorithms and then iteratively extract those candidates, calculate for each a detection significance statistic (probability of the null hypothesis that all the X-rays found in the source aperture arose from the background), and prune candidates found to be not significant. Our scientific goal to push for high sensitivity, accepting a non-trivial number of spurious detections (Broos et al. 2011a). The AC08 catalog was defined using a different algorithm (Palermo wavelet detection code, PWdetect; Damiani et al. 1997) and more conservative thresholds that are expected to produce only  $\sim 10$  spurious detections within the ACIS-I field of view.

Broos et al. (2011a) discuss why estimating the number of false detections in the CCCP catalog or in the Trumpler 16 study region is not practical, and point out that such an estimate would be irrelevant for any analysis that further restricts the sample of stars, e.g., by requiring a “likely member” classification or requiring an estimate of X-ray luminosity from XPHOT. However, an approximate *lower limit* on the number of legitimate X-ray sources in any sample can be obtained by tallying the number NIR counterparts identified. Among the 1232 CCCP sources in our study area, 1067 (85%) have NIR counterparts detected in at least one band. Among the 1187 classified

as likely Carina members, 1047 (88%) have NIR counterparts; among the 885 with X-ray luminosity estimates, 804 (91%) have NIR counterparts. Since we have confidence that X-ray sources bright enough for XPHOT photometry are real astrophysical sources, this limits the total fraction of false positives to a few percent of the faintest X-ray sources and hence should not effect any conclusion.

### 3. Results: Global Considerations

Structurally, Tr 16 is a roughly circular cluster about  $11'$  across (7.4 pc at 2.3 kpc). We also consider the Southeastern extension to be part of the cluster (Figure 1). Table 1 enumerates the 1232 X-ray sources within the continuous contour with  $> 1$  X-ray source per  $30''$  kernel. Of these, the X-ray hardness and other criteria (Broos et al. 2011) classify 1187 as probable members of the Carina complex, 11 as foreground objects, 2 as extragalactic and 32 unknown. We find 392 sources not in the original catalog of AC08. Most of these are faint sources: the mean number of net counts in these new sources is 7 and the minimum is 2.3. About 50 are found in the Southeastern extension which was not fully included in ObsID 6402. The median energy of the previously detected sources is indistinguishable from the newly detected sources,  $MedE \simeq 1.5$  keV. The penultimate column of Table 1 lists the class of the X-ray source following Broos et al. (2011) H0: unclassified; H1: source is a foreground main-sequence star; H2: source is a young star, assumed to be in the Carina complex; H3: source is a Galactic background main-sequence star; H4: source is an extragalactic source. The final column of Table 1 indicates the sub-cluster with which the source is identified (C3 = Sub-cluster 3 etc.) based on the nomenclature in Paper I. We also identify those stars which are not identified with any single cluster as being part of the ‘matrix’ of Trumpler 16. The matrix stars in the Southeastern extension are identified separately as “SEM”.

#### 3.1. Disk Fraction

For the 1187 X-ray sources found to be probable members of the Carina complex, matches are found in the HAWK-I photometric catalog for 1047. Almost all of those (1032 sources) are detected in all three  $JHK$  bands. The bulk of the X-ray sources matched have  $12 < K_S < 15.5$  with wings extending to both brighter and fainter sources. Of the 1032 ,probable members of the Carina complex with JHK detections, 1013 sources have errors less than 5% in all bands. Ninety of 1013 ( $8.9\% \pm 0.9\%$ ), have excesses consistent with an optically thick disk (Figure 2). This is a slightly higher rate than the 7.8%, found for the full CCCP by Preibisch et al. (2011) or the 6.9% disk detections they found for the 529 X-ray sources located in the Trumpler 16 sub-clusters. The sources reported by Preibisch et al. are a sub-sample (only the sources which reside in sub-clusters) of the whole of Trumpler 16 which we covered here. Also, we require a  $K_S$  excess to be 10%, this is higher than the Preibisch et al. study, but is closer to the value used by AC08 who reported a relatively high disk fraction of  $\sim 15\% \pm 2\%$ .

In AC08, the sample is restricted to the 339 2MASS sources with good colors in all three bands. The true limiting factor for inclusion is the  $K_S$  band magnitude which needs to be brighter than about 15. Sources without a  $K_S$  band excess are more likely to be excluded from the 339 stars sample, which will raise the disk fraction. In the present study the IR data are more complete than the X-ray data, so we do not expect a strong IR bias in favor of detecting stars with disks.

### 3.2. IR magnitude and X-ray Flux

As seen in Figure 3, the X-ray fluxes of the sources are well correlated with  $J$ -band luminosities for  $6 < J < 11$ . This relation appears to reverse between  $12 < J < 14$  and reappears in the range  $14 < J < 18$ . Below  $J=18$  the flux distribution appears flat. Most of this can be readily interpreted as follows. Given the 2.3 kpc distance and a roughly 3 Myr age, objects with  $6 < J < 11$ , are primarily high-mass stars, which generate X-rays through shocks in unstable radiatively driven winds (Lucy 1982). Both the luminosity and the shock speeds scale with mass down to early-B stars (See the Nazé et al. 2011 in this issue). Similarly, objects with  $14 < J < 18$  are pre-main sequence (PMS) G, K through mid-M stars that are known to have their bolometric luminosity correlate with their X-ray luminosity. This is seen for example, in the Chandra Orion Ultradeep Project (COUP) study of the Orion Nebula Cluster (Preibisch et al. 2005). For these stars, roughly 0.02% of their luminosity is emitted in X-rays although the overall fraction can be higher during X-ray flares. Below  $J=18$ , typical PMS stars are too faint to be detected in these observations and only those caught during strong flares are seen.

The behavior between  $12 < J < 14$  is curious. For the 2.3 kpc distance and  $\sim 3$  Myr age these are Mid-B through A stars, which are not efficient X-ray producers since they have weak winds, but  $\sim 30 - 60\%$  of such stars in Trumpler 16 and COUP were detected in X-rays (Evans et al. 2011; Stelzer et al. 2005). Both Evans et al. and Stelzer et al. concluded that high energy emission from these sources originates in unseen companions. It has not previously been reported that the X-ray flux became brighter as the stars became bolometrically fainter. Previous samples were probably too small to detect this effect. If the X-ray emission was indeed the result of unseen companions, the implication is that the higher mass primaries (B5-A5) typically have lower mass companions than the primaries below A5.

To quantify these effects, we performed a piecewise least-squares linear regression and applied nonparametric correlation measures to the data in Figure 3. The fitted slope is  $m = -0.76 \pm 0.05$  for  $6 < J < 10$ ,  $m = -0.30 \pm 0.02$  for  $14.5 < J < 17$  but reverses direction to  $m = 0.18 \pm 0.08$  for  $12 < J < 14$  (these lines are plotted in Figure 3). Kendall’s  $\tau$  correlation coefficient (Kendall 1938) gives  $\tau = -0.86$  for the bright stars,  $-0.41$  for the faint stars, and  $0.21$  for the intermediate brightness stars. The probability for the correlation of the intermediate stars is  $P \sim 0.5\%$ , roughly equivalent to a  $3\sigma$  effect.

Because we found the effect surprising we repeated the tests, allowing the limits on the inter-

mediate J magnitude band to vary by up to 0.5 mag. We also calculated probabilities in various terms including the Spearman  $\rho$  correlation coefficients (Spearman 1904) for each these are -0.70 for the bright J band sources, -0.30 for the fainter J band sources and 0.13 for the intermediate case. In all cases, there is a weak positive correlation in the middle range. Further, a similar pattern has been seen in the Trumpler 14 and Trumpler 15 clusters within the  $\eta$  Carina cluster (Evans et al. *in prep*). No correlation is seen when the entire CCCP sample is used, however this sample covers relatively broad range of ages and conditions.

### 3.3. Near-IR Extinction

We originally calculated extinction to each source following  $\tilde{A}_V = (H - K_S - 0.1) \times 13.7$  (Preibisch et al. 2011).<sup>1</sup> Preibisch et al. note that  $\tilde{A}_V$  calculated in this manner may not be accurate for all masses: the first term assumes stellar photospheric color  $H - K_S = 0.1$  appropriate for 3 Myr stars between 1-2  $M_\odot$  (Siess et al. 2000). Below 1  $M_\odot$ , photospheric  $H - K_S$  exceeds 0.1 and extinction is over-estimated, and above 2  $M_\odot$ , extinction is underestimated. This can lead to estimates of negative extinction. To minimize these effects, we only estimate extinction for stars with no evidence of optically thick disks at  $K_S$  and  $J$  magnitudes between 14.5 and 16.5 as these are likely to have masses of 1– 2  $M_\odot$ .

The second term is the proportionality factor characteristic of the extinction law. We note the derived reddening law measured for this region appears to deviate from the typical ISM value of  $R=3.1$ , with derived values being between 3.8 and 5 with possible spatial variations (Nazé et al. 2011, Povich et al. 2011, Gagné et al. 2011, Smith 1987, Thé 1980, Herbst 1976, Forte 1978, Feinstein et al. 1973). However, using only optical data, Turner & Moffat (1980) found  $R = 3.2$  throughout the Carina region. He we us  $\tilde{A}_V/E_{(B-V)}=4.0$  (Povich et al. 2011) which leads to the constant values  $k=13.7$ . A higher value of  $R_V$  would lower the value of  $k$ . Given these constraints, we find the mean  $\tilde{A}_V = 3.8$  with 25% and 75% quartiles at 2.9 and 5.0, respectively, for the Trumpler 16 CCCP sample of likely Carina members.

AC08 calculated extinction by using a  $K_S$  vs.  $J - H$  color-magnitude diagram, individually dereddening stars until the location of the star intersected the isochrone for a 3 Myr cluster PMS (isochrones from Siess et al. 2000). They found a mean reddening of  $A_V=3.6\pm 2.4$  mag, acknowledging that their estimates of  $A_V$  could be in error by up to 0.7 mag due to the relatively high photometric errors in the 2MASS data. While overall this method is more precise than that used by Preibisch et al. (2011), the errors may be higher than estimated due to their unconfirmed assumption that all stars are exactly 3 Myr old. Furthermore, we expect our data to be deeper and hence capture more highly extinguished stars than the 2MASS sample. Another important aspect

---

<sup>1</sup>Following Preibisch et al. we use the expression “ $\tilde{A}_V$ ” to indicate extinction calculated using this simple scaler relation. We use “ $A_V$ ” to indicate extinction measurements obtained by individually fitting a given stellar color + extinction to a model color in this case using Siess et al. (2000).

for the comparison of HAWK-I and 2MASS is the spatial resolution: about 2 arcsec for 2MASS versus about 0.6 arcsec for HAWK-I. Many "point-like" 2MASS sources are resolved into several components in the HAWK-I images. Other effects such as photometric variability of the young stars, unresolved binary companions, and small infrared excesses (that are too small to move the star out of the main-sequence reddening band in the color-color diagram) will all add both random and systematic errors into the extinction measurements.

We examined a sub-sample of about 100 stars with non-degenerate<sup>2</sup> reddening extinctions measured by AC08. We find an offset  $\Delta = 0.58$  mag between the mean value for  $\tilde{A}_V$  obtained here and the mean  $A_V$  published by AC08. The latter tends to show less extinction. There is considerable scatter between the two  $\tilde{A}_V$  estimates,  $\sigma = 1.0$ . When we restrict the sub-sample further to 65 stars with extinction corrected magnitudes of  $13 < K_S < 14$ , which would place their masses between 1 and 2  $M_\odot$ , the difference and dispersion are reduced to  $\Delta = 0.4$  and  $\sigma = 0.8$ . This indicates that extending the simple correction used by Preibisch et al. beyond its designed range caused some of the scatter. We then calculated extinctions for each source, following the methods described by AC08, but using the HAWK-I data and found that large scatter and systematic offsets around  $A_V \simeq 0.5$  persist.

Considering all factors – ranges in age, measurement errors, mass limitations, dust particle size distribution – the level of agreement between the different methods appears reasonable. Since the assumption of intrinsic  $H - K_S = 0.1$  is accurate to within 3% for stars with masses  $2.2 > M_\odot > 0.8$  which dominate the X-ray distribution, the extinction estimator of Preibisch et al. (2011) seems appropriate for the CCCP Carina member sample exclusive of the O, B and A stars.

In Figure 4 we show the  $J$  vs.  $J - H$  color-magnitude diagrams for Trumpler 16 and several of the sub-clusters. The solid (green) line on the left hand side of the plot is an isochrone from Siess et al. (2000) assuming an age of 3 Myr and a distance modulus of 11.81. We can globally fit the extinction to the cluster, by dereddening the ensemble of stars with  $13 < J < 17.5$  in steps of 0.1  $J$  magnitudes and measuring the  $\chi^2$  residuals versus the 3 Myr isochrone model. We restricted the sample to stars without evidence for optically thick disks. The best fit was found for an extinction value of  $A_V=3.3$  with interquartile confidence band of 2.3 – 3.8. When the sample is restricted to 1–2  $M_\odot$  likely Carina members, the mean becomes  $A_V = 4.1$  with interquartile range 3.4 – 4.9.

### 3.4. X-Ray Absorption

Individual X-ray luminosity and absorption were calculated for X-ray sources in the direction of Trumpler 16 using the XPHOT package (Table 2; Getman et al. 2010). The concept of the XPHOT

---

<sup>2</sup>When calculating infrared extinctions for 3 Myr stars, the reddening vector crosses isochrones multiple times for stars with masses between about 2.2-8.0  $M_\odot$ . For these stars, IR data alone are not conclusive and we identify the reddening determinations as degenerate.

method is similar to the use of color–magnitude diagrams in optical and infrared astronomy, with X-ray median energy replacing color index and X-ray source counts replacing magnitude. Using non-parametric methods, one can estimate both apparent and intrinsic broadband X-ray fluxes and soft X-ray absorption from gas along the line-of-sight to X-ray sources. Apparent flux is estimated from the ratio of the source count rate to the instrumental effective area averaged over the chosen band. Absorption, intrinsic flux, and errors on these quantities are estimated from comparison of source photometric quantities with those of high signal-to-noise spectra that were simulated using spectral models characteristic of low-mass pre-main sequence stars. In the original paper, the results were compared with spectroscopic analysis of sources in M 17 (Broos et al. 2007). For stars with median total band energy  $> 1.7$  keV, Getman et al. (2010) show that fluxes measured by XPHOT agree with fluxes obtained by spectral fitting to within a factor of  $\sim 1.5$  for sources with more than 50 counts, and within a factor of  $\sim 4$  for sources with as few as 10 counts. The total band covers the 0.5 – 8.0 keV energy range.

For the Trumpler 16 sample, 347 sources could not be assigned a flux or temperature. Eighty percent of these had less than 10 counts and all but six had less than 30 counts. The final six had photon distributions inconsistent with the model of a one-temperature  $\sim 1.5$  keV corona. The remaining 885 sources had X-ray luminosity and absorption calculated. For sources with between 10–20 counts, the median error in total flux in total flux is about 35% and the statistical error in  $N_{\text{H}}$  is also about 35% (for median energy of 1.5 keV). In the lowest count bin, 5–7 counts, the median error in total flux in total flux is about 65% and the statistical error in  $N_{\text{H}}$  is also about 45% (for median energy of 1.5 keV). There is also a systematic error on the  $N_{\text{H}}$  value due to low effective area below about 500 eV. The systematic error is about 15% at 1.5 keV but approaches unity for sources below 1 keV. The converse of this is that ACIS spectral resolution is not fine enough to discriminate  $\log N_{\text{H}}$  values significantly below 22.0 (Getman et al. 2010). Below  $\log N_{\text{H}}=21.6$  systematic errors dominate over statistical errors with a median statistical error in  $\log N_{\text{H}}$  of about 0.3 and systematic errors as high as  $\log N_{\text{H}}=1.15$ . Above  $\log N_{\text{H}}=21.6$  statistical errors dominate with a median statistical error in  $\log N_{\text{H}}$  of about 0.2 but statistical errors still as high as  $\log N_{\text{H}}=1.0$ . It is cautioned that  $\log N_{\text{H}}$  values below 21.6 are less robust than high values of  $N_{\text{H}}$ .

The mean  $N_{\text{H}}$  value derived from XPHOT results here is essentially identical (within 10%) to that found by AC08 using other methods. However, we find a systematic bias between XPHOT and XSPEC  $N_{\text{H}}$  values for the stronger X-ray sources in Trumpler 16 in the sense that for  $\log N_{\text{H}}(\text{cm}^{-2}) \leq 21.75$ , XPHOT gives a larger value and for  $\log N_{\text{H}}(\text{cm}^{-2}) > 21.75$  XSPEC gives a higher value. At the extreme values, the differences can be 0.75 dex. This finding is consistent with the result in Getman et al. (2010) wherein the observed median energies of stellar sources in M 17 were found to have a simple linear relation to the  $\log N_{\text{H}}$  for values of  $\log N_{\text{H}}(\text{cm}^{-2}) > 21.6$ . The XPHOT derived absorptions were deemed unreliable for 205 sources with  $\log N_{\text{H}} < 21.6 \text{ cm}^{-2}$  and below a median energy of 1.7 keV, due to degeneracy in the median energy –  $\log N_{\text{H}}$  relationship used by XPHOT.

Figure 5 shows the distribution of absorption columns found by XPHOT for the sources in the direction of Trumpler 16. The distribution is highly structured, especially when compared to Figure 7 of AC08. About 5% of the sources have  $\log N_{\text{H}} < 21$ ; some of these may be Galactic field foreground stars misclassified as likely Carina members. About 15% of the CCCP likely Carina members have  $21.2 < \log N_{\text{H}}(\text{cm}^{-2}) < 21.6$ , leading to a strong peak in the distribution of sources at  $\log N_{\text{H}} \simeq 21.7 \text{ cm}^{-2}$ , with a similar shoulder around  $22.0 < \log N_{\text{H}}(\text{cm}^{-2}) < 22.3$ . A small number of sources have higher absorptions in the range  $22.3 < \log N_{\text{H}}(\text{cm}^{-2}) < 23.4$ ; some of these may be embedded Carina protostars, while others may be misclassified extragalactic sources.

If the very low absorption tail ( $\log N_{\text{H}}(\text{cm}^{-2}) < 21.0$ ) is attributed to foreground contaminants, then the distribution of X-ray absorptions has a strongly peaked unimodal distribution very similar to the distribution of absorptions derived from IR photometry (Figure 4). Using the conversion  $N_{\text{H}} = 1.6 \times 10^{21} A_{\text{V}} \text{ cm}^{-2}$  obtained by Vuong et al. (2003), the peak of the Trumpler 16 X-ray absorption distribution is equivalent to  $A_{\text{V}} \simeq 3 \text{ mag}$ , in agreement with the value  $A_{\text{V}} \simeq 3 - 4 \text{ mag}$  obtained from the near-IR color-magnitude diagrams (§ 3.3). Both the X-ray and IR absorption distributions have a sparse tail of extinctions found going out to  $A_{\text{V}} > 30 \text{ mag}$ .

### 3.5. X-ray Luminosity Distribution

As most of the CCCP sources in Trumpler 16 are too faint in the X-ray band for direct spectral modeling (Figure 6), the XPHOT technique is used to scale the observed count rate to broad-band luminosity with a correction for soft X-ray absorption. Getman et al. (2010) find that most XPHOT total-band fluxes are within  $\pm 20\%$  of values determined with XSPEC for the absorption ranges typically seen in the Trumpler 16 region. They estimate the errors in total-band source fluxes to be better than 60%, 50%, 30%, and 20% for net count strata 7–10, 10–20, 20–50, and >50 counts, respectively, with a small systematic bias. In Trumpler 16, nearly 500 of the 885 sources with fluxes and luminosities measured by XPHOT have less than 7 net counts. The simulations estimate less than 70% errors for these sources.

As noted by Feigelson et al. (2005), the X-ray luminosity function (XLF) is the product of the initial mass function and the correlation between mass-age and X-ray luminosity. This correlation is well-studied in the COUP and Taurus young stellar populations (Preibisch et al. 2005, Telleschi et al. 2007). The X-ray luminosity functions of the ONC, IC 348, NGC 1333 and other young clusters appear similar, suggesting that the XLF shape may be roughly “universal” (Wang et al. 2008). For the youngest clusters, differential evolutionary effects appear minimized and the XLFs of the clusters are well fitted by a log-normal function with  $\langle \log L_{\text{X}} \rangle (\text{erg s}^{-1}) = 29.3$  and  $\sigma = 1.0$  (Feigelson et al. 2005). Wang et al. (2008) find some deviations from precise agreement for different clusters; for example, a steeper slope in the XLF of M17 and a more shallow slope for the Cep OB3b cluster is seen. Meanwhile M17 has nearly 3 times the stars of the ONC while Cep B less than half the unobscured population of the ONC (Broos et al. 2007, Getman et al. 2005, 2006). The implication is that more massive clusters may have a steeper slope to their luminosity function.

Figure 7 compares the XLF of Trumpler 16 (excluding the SE extension) with the XLF of the COUP data (Getman et al. 2005). To determine the XLF of Trumpler 16, the first step is to estimate the completeness of the X-ray data. Figure 7b shows a histogram of the luminosity as derived by XPHOT of 687 X-ray sources observed in Trumpler 16 (this is down from 885 because we are excluding the SE extension which has different properties as will be discussed in § 4). Visual examination of Figure 7b shows a drop off starting at  $\log L_{t,c} = 30.5$  ( $L_{t,c}$  = absorption corrected luminosity in the total band covering 0.5 - 8.0 keV). This value is consistent with the CCCP completeness limits discussed by Broos et al. (2011a), which vary strongly with off-axis distance and with absorption. The implication is that incompleteness in the distribution occurs before this point, mostly before  $\log L_{t,c} = 30.7$ .

As shown in Figure 7a, we fitted the cumulative XLF of Trumpler 16 (excluding the SE extension) with a power-law between  $\log L_{t,c} = 30.7 - 31.5$  and find a slope  $\Gamma = -1.27$ . This slope was sensitive to the lower luminosity cut-off used at the level of 0.05 in slope for a 20% change in the luminosity limits;  $\Gamma = -1.13$  if we brought the lower cut-off down to  $L_{t,c} = 30.3$  which is clearly incomplete. The upper cutoff of  $L_{t,c} = 31.5$  is essentially the brightest cool star. This slope is steeper than a similarly measured slope for the COUP data which is found to be  $\Gamma = -0.93$  for  $\log L_{t,c} = 30.2 - 31.5$ . The slope of the COUP data is less sensitive to the lower luminosity cut-off and is only effected at the level of 0.01 for a 20% change in the luminosity limits.

To estimate the total number of sources in the cluster, we simply compare the total number of sources in Trumpler 16 to the number in the COUP sample in the range from  $\log L_{t,c} = 30.7 - 31.5$  which should be dominated by cool stars. The COUP sample contains 51 sources in this range, while the Trumpler 16 sample has 255 for a factor of  $5(\pm 0.5)$  more. Given an estimate for the total population of the ONC from the COUP as 1300 X-ray sources (Getman et al. 2005) we estimate the total population of Trumpler 16 at  $6500 \pm 650$  if observed to a similar X-ray luminosity limit. Further, Hillenbrand & Hartmann (1998) estimate the overall ONC population to be 2800. If this is correct, then the X-ray sources represent less than 50% of the total cluster membership which may be as high as 14,000.

#### 4. The Sub-clusters within Trumpler 16

Paper I defines Trumpler 16 as a region in which the surface density of CCCP likely Carina members smoothed with a  $30''$  Gaussian kernel (FWHM=0.8 pc) exceeds 1 source per kernel. Within this region, Paper I identified seven sub-clusters within Trumpler 16 with sub-cluster surface density exceeding three sources per  $30''$  Gaussian kernel. Overall, Paper I finds 31 small X-ray selected groups of probable Carina members in the CCCP. Trumpler 16 contains 8 of these groups, including one in the Southeastern extension, which we refer to as sub-clusters. No single sub-cluster exceeds 15% of the total number of sources in the Trumpler 16 cluster. The exact number and shape of these sub-clusters varies depending on the smoothing kernel the density factor. This is unlike Trumpler 14 and 15 which are each dominated by a single, central concentration.

In this section, we examine whether the sub-clusters are physically distinct units or simply statistical fluctuations, and we compare their properties. The sub-cluster identification for each source is given in Table 1 and Figure 8. In the figure, we have approximated each sub-cluster as an ellipse to aid in the calculation of geometric parameters. For each sub-cluster we have assessed extinction as  $\tilde{A}_V$  for stars of  $K_S < 13$ . We then applied the extinction to the observed  $K_S$  magnitude and the distance to produce a K-band luminosity function (KLF). As discussed above, the actual values of individual stars are not reliable and may be in error by up to 0.2  $K_S$  mag., but the structure of the distribution should be representative. To quantify the structures, we have identified the quartile values of absolute  $K_S$  and  $\tilde{A}_V$  for all sub-clusters.

In order to determine if the sub-clusters truly stand out from the background cluster population of Trumpler 16, we first look at the 506 X-ray sources which form the matrix of Trumpler 16. These are cluster members, but not coincident with any specific sub-cluster, nor the Southeastern extension. Of the 438 sources with good mid-IR colors, 6.4% ( $\pm 1.2\%$ ) show IR excesses consistent with an optically thick disk. This is more than  $2\sigma$  less than the cluster as a whole and may indicate that these dispersed stars are more evolved than the global population. The mean extinction value of  $\tilde{A}_V = 3.8$  is indistinguishable from the cluster as a whole.

#### 4.1. Sub-cluster 3

Sub-cluster 3 is the westernmost of the Trumpler 16 sub-clusters. When a larger smoothing kernel is used, it appears as a low density extension of Sub-cluster 6. It contains 33 X-ray sources and has a spatially averaged source density of  $32 \text{ src pc}^{-2}$ . Twenty-seven of the X-ray sources have been matched with HAWK-I sources; almost all of these are between 1 and  $2 M_\odot$ . About  $15\% \pm 7\%$  of the IR detected X-ray sources have disks. The mean  $\tilde{A}_V$  is 3.8 similar to the cluster as a whole. The massive supergiant Tr 14 Y 398 (spectral type O3 Iab) as well as WR 25 (HD 93162, WN) lie on the western edge of the sub-cluster.

#### 4.2. Sub-cluster 4

Sub-cluster 4 is the smallest of the Trumpler 16 sub-clusters with only 11 X-ray sources. The spatially averaged source density of  $36 \text{ src pc}^{-2}$  is about the same as Sub-cluster 3. Of the eight X-ray sources matched to HAWK-I, two have  $K_S$  excesses consistent with an optically thick disk. The mean  $\tilde{A}_V$  is 3.5. The B1 V star CPD–59°2581 lies near center of the sub cluster, and the similar B1 V CPD–59°2574 at the northwestern edge of the sub-cluster. Neither of these stars were detected in X-rays.

### 4.3. Sub-cluster 6

Sub-cluster 6 is a centrally condensed sub-cluster and the second largest in Trumpler 16 overall with 109 sources and an average source density of  $45 \text{ src pc}^{-2}$ . Of the 88 sources with good mid-IR colors,  $6.8\% \pm 2.8\%$  show IR excesses from an optically thick disk, consistent with the global population. Sub-cluster 6 has a similar absorption to the previously discussed regions with mean  $\tilde{A}_V = 3.6$  and 75% quartile  $\tilde{A}_V = 4.1$ . There are three O stars in this sub-cluster, the O3.5 V+ O8 V double HD 93205 and an O5 V HD 93204. These are displaced by 0.25 pc to the southwest of the cluster center.

### 4.4. Sub-cluster 9

Sub-cluster 9 is the western half of a bow-tie shaped enhancement toward the southern part of Trumpler 16. The 53 sources appear uniformly distributed with no internal concentrations and a high spatially averaged source density of  $48 \text{ src pc}^{-2}$ . The X-ray sources here are relatively faint, about half of the sources in the region required the more sensitive source detection procedure described by Broos et al. (2010) and were not found by AC08. This is about twice the usual fraction of newly identified sources. Of the 45 sources with good mid-IR colors, only 2 ( $4\% \pm 3\%$ ) show IR excesses consistent with an optically thick disk. One of these is exceptionally faint,  $K_S = 19.5$  and hence the colors are quite dubious. The mean extinction calculated for the region as a whole is typical of other regions with  $\tilde{A}_V = 3.7$ . There are no high-mass stars in this region.

### 4.5. Sub-cluster 10

Sub-cluster 10 is the eastern half of the bow-tie shaped enhancement toward the southern part of Trumpler 16. The 82 sources appear uniformly distributed with no strong internal concentrations and a high spatially averaged source density of  $42 \text{ src pc}^{-2}$ . The X-ray luminosity is more typical here, 20% of the sources required the more sensitive source detection procedure described by Broos et al. (2010). Of the 74 sources with good mid-IR colors, only 4 ( $5.4\% \pm 2.7\%$ ) show IR excesses consistent with an optically thick disk. Two of these are faint,  $J > 18.1$  and hence the colors have errors of about 35%. Thus there are only two bona-fide disk systems in this subcluster. The mean extinction calculated for the region as a whole is typical of other regions with mean  $\tilde{A}_V = 3.7$ . Four late O stars in the region are all detected in X-rays. The most massive, O7 V star CPD–59°2626, lies near the subcluster center, while the others lie towards the east and southeast.

Although sub-clusters 9 and 10 are in contact, they have different mass distribution. Sub-cluster 9 has fewer higher mass stars. Both clusters have relatively low numbers of stars with optically thick disks in the  $K_S$  band.

#### 4.6. Sub-cluster 11

$\eta$  Carinae and 6 other high-mass stars reside in sub-cluster 11. The 71 X-ray sources include five of the high mass stars. Overall the X-ray sources are centrally condensed with a peak at 10:45:06 –59:40:25, about 0.3 pc from  $\eta$  Carinae. The spatially averaged source density of 27 src pc<sup>-2</sup> is among the lowest of any region. This may be due, in part, to reduced point source sensitivity in the immediate vicinity of  $\eta$  Carinae and the associated X-ray nebula. Of the 57 sources with good mid-IR colors, 4 show IR excesses consistent with an optically thick disk (7%± 4%). The mean extinction calculated for the region as a whole is low,  $\langle \tilde{A}_V \rangle = 2.9$ .

#### 4.7. Sub-cluster 12

Sub-cluster 12 is immediately to the south of sub-cluster 11, centered at 10:45:10.6, –59:42:54. It is the most centrally condensed and populous sub-cluster of Trumpler 16 with 166 X-ray sources. It includes six of the nine most massive stars in Trumpler 16. There are two high-mass stars within 15" of the center, both of which are early B stars, not O stars. The most massive star complex in the cluster, CPD–59°3310, contains two high-mass stars, an O6 V + a B2 sub-giant, and is located about 2' to the southeast of the cluster center. An additional candidate OB star at the center of sub-cluster 12 is identified by Povich et al. (2011). This is the only one of 94 new OB star candidates in the CCCP located within the main area of Tr 16 (three were identified around the periphery and five in the Southeastern extension).<sup>3</sup> The spatially averaged source density is 45 src pc<sup>-2</sup>. Of the 142 sources with good mid-IR colors, 10.6% ± 2.7% show IR excesses consistent with an optically thick disk. All but one of these are found at relatively high extinction ( $A_V > 2.6$ ), indicating they likely lie behind a source of extinction within the sub-cluster. Further, the cumulative extinction distribution is very steep, with 60% of the X-ray sources with  $3.4 < \tilde{A}_V < 4.2$ . All the disked stars are among the most absorbed 15%. It appears there is a thin cloud with  $\tilde{A}_V \sim 1$  near the front of this sub-cluster. Figure 9 shows the extinction functions of several regions within Trumpler 16, with sub-cluster 12 showing the steepest distribution.

#### 4.8. The Southeastern Extension and Sub-cluster 14

To the southeast of the main body of Trumpler 16, separated by a dust lane, is a continuation of the density distribution which we identify with Trumpler 16. This region was first recognized by Sanchawala et al. (2007a, b) who identified 10 X-ray sources in this region using the first two *Chandra* observations of the Carina nebula (ObsIDs 1249 and 50). The region is distinguished by high extinction,  $\langle A_V \rangle = 4.2$ , and a steep KLF indicating a young age. Using the larger CCCP

---

<sup>3</sup>There is also a strong selection effect as the Spitzer VelaCarina survey was highly constrained when observing near  $\eta$  Carinae.

mosaic, we find this extension covers about 40% of the area of the main cluster and contains 156 X-ray sources. The bulk of this extension was outside the field of ObsID 6402 and has somewhat lower overall exposure time, about 60 ks rather than 90 ks. Hence, a lower surface density of sources is expected. Even in light of the difference in exposure times, it is clear that conditions are different in this region. The disked fraction is much higher than the rest of the cluster,  $19 \pm 4\%$ .

Within the Southeastern extension, there is a density enhancement identified as sub-cluster 14 in Paper I. This corresponds with the location of the 10 X-ray sources identified by Sanchawala et al. (2007a, b). We find 40 stars within this sub-cluster and a very high extinction,  $\langle \tilde{A}_V \rangle = 7.4$ . Sub-cluster 14 is identified as a more embedded region within the Southeastern extension. This sub-cluster also has the highest disked fraction,  $21 \pm 8\%$ , of any sub-cluster with a significant number of stars. The eclipsing O5.5 + O9.5 binary V662 Carinae is located within about  $15''$  (0.1 pc) of the cluster center making sub-cluster 14 the only one of the eight sub-clusters with a dominant O star so close to its geometric center. Four of the five OB candidates identified by Povich et al. (2011) in the Southeastern extension lie within sub-cluster 14. Three rank among the seven most luminous of all the OB star candidates in the CCCP.

The matrix of stars surrounding sub-cluster 14 is composed of 116 X-ray sources in the region, including the O4 V star LS 1886 located in the eastern portion of the extension. Removing sub-cluster 14 from the Southeastern extension, the region still stands out with high extinction  $\langle \tilde{A}_V \rangle = 4.8$  and a high disked fraction of  $18 \pm 4\%$ .

#### 4.9. Discussion of Sub-clustering

The metrics for each sub-cluster are summarized in Table 3. It is clear that the main body of Trumpler 16 (subclusters 3, 6, 9, 10, 12 and the surrounding matrix) is different from the Southeastern extension. The extinction is nearly 3 magnitudes greater in the Southeastern extension and the disked fraction is more than twice that of the main body. Within the Southeastern extension, sub-cluster 14 is distinguished by an additional 2 magnitudes of extinction in the V band and a higher disked fraction. The disk fraction can be used as a proxy for age (Haisch et al. 2001). While the age calibration is sensitive to the sensitivity of the survey, disked fraction appears to decrease nearly linearly in time – indicating that the Southeastern extension is about 80% the age of the main body of Trumpler 16.

Within the main body of Trumpler 16, the sub-clusters appear to be dynamically distinct structures. Some have  $> 100$  stars with surface densities  $> 3$  times that of the outer portions of the matrix, too rich to arise from statistical fluctuations. On the other hand, except for chance difference in line-of-sight absorptions with respect to Carina clouds, the X-ray selected stars in the sub-clusters are similar to each other and to the stars in the matrix. Stars in all of the sub-structures outside of the SE extension have disk fractions consistent with  $\sim 7\%$ . The stars in the matrix tend to have a slightly lower disk fraction than the stars in the sub-clusters but the significance is  $< 2\sigma$ .

The massive O stars, both main sequence and supergiant, do not lie at the cores of the sub-clusters. Few young stellar clusters are documented to have widely distributed massive stars; the best example may be NGC 2244, the central cluster in the Rosette Nebula (Wang et al. 2008).

## 5. The Relation of the High-Mass Stars to the Sub-clusters

X-ray emission is detected from 29 stars in Trumpler 16 that were classified with spectral types earlier than B2 (Skiff 2010). This includes  $\eta$  Carinae itself, which was detected, but not cataloged by Broos et al. (2011) due to its high degree of pile-up (saturation in the ACIS CCD detection) which makes characterization difficult. The remainder include WR 25 and 19 O stars, many of which are in multiple systems. In addition, there are eight B stars in the range from B0.5 to B2 which were detected in X-rays, six of these with less than 15 net counts.

There are 21 early-type stars which were not detected in the X-ray observations. Most of the non-detections are from B0V to B2V in spectral type. This indicates a very sharp drop off in X-ray activity across the O/B divide as all the O stars were detected. There were also a few early-type stars not detected in X-rays which were also not considered to be main sequence either. All of these are in the far south and all but emission object Hen 3-480 are considered to be part of the Southeastern extension. We list the detections in Tables 4 and 5 and the non-detections in Table 6. More comprehensive studies of early-type stars are the topics of separate papers in the framework of the CCCP (e.g., Nazé et al. 2011; Gagné et al. 2011). Candidates from Povich et al. (2011) are excluded from this discussion as well since followup is still required to establish their spectral types and confirm their OB status.

Following the finding of AC08 that OB stars are less absorbed than their late type counterparts ( $A_V=2.0$  for OB stars versus 3.6 for GK stars), we examine the extinction to the X-ray detected early-type stars. Twenty-five of these have matches in the HAWK-I photometry catalog. We calculated the extinction by comparison to the  $J - H$  and  $J - K_S$  colors of high-mass stars which are expected to be nearly constant at  $-0.15$  and  $-0.2$  respectively, in the absence of extinction. We find a range of extinctions from  $A_V \sim 0.85 - 8.9$ . The average  $A_V$  is about 2.5 but this is dominated by a single outlier (MJ 224) with  $A_V \sim 8.75$ . The mean extinction may be the more appropriate metric at  $A_V \sim 2.1$ . However the dispersion is high,  $\sigma = 1.0$  even excluding the outlier. Hence, the extinction of the high-mass stars is generally lower than that of the low-mass population. The single high mass member of the Southeastern extension detected in X-rays has  $A_V \sim 4.5$  consistent with membership in Sub-cluster 14.

Remarkably, the spatial distribution of the high-mass stars does not follow the sub-clustering seen in the lower mass stars. None of the seven sub-clusters in the main body of Trumpler 16 has an O star within 0.2 pc of the cluster center; this includes sub-cluster 11 – the host of  $\eta$  Carinae. The centroid of the X-ray sources in this sub-cluster is located  $0.7'$  (0.5 pc) from  $\eta$  Carinae. The unclustered matrix has the same fraction of high-mass stars to lower mass stars. Only Sub-cluster 14

in the Southeast extension appears centered on a high mass star.

## 6. Trumpler 16 in Context

In Paper I, it is shown that the Carina nebula has very complex clustering properties including many sparse groups, a few small clusters such as Bochum 11 and the “Treasure Chest,” as well as three large clusters, Trumpler 14, Trumpler 15, and Trumpler 16. This range of stellar groupings is seen in other large star forming regions such as the Orion A cloud, which includes the ONC, OMC 2/3, Lynds 1641 North, Lynds 1641 South, as well as numerous small agglomerations. But comparison of the three largest clusters implies something other than size matters.

In Table 7 we provide a direct comparison of the clusters. The data sets are not analyzed in identical ways but the methods are comparable. Trumpler 14 appears to be the youngest of the three clusters as determined by a variety of metrics including the location of the stars on the color–magnitude diagram and the disk fraction. It also possesses the most X-ray sources and is most centrally condensed. In this Table we calculated the total number of stars in Trumpler 14 based on the total mass estimate of 9000–11,000  $M_{\odot}$  of stars by Ascenso et al. (2007) and then estimating the mean stellar mass to be 0.8  $M_{\odot}$  following Hillenbrand & Hartmann (1998). Ascenso et al. estimate the distance to the Carina nebula to be 2.8 kpc, not the 2.3 kpc used here, so the total number of stars should be estimated to be perhaps 10% larger. The densities shown in Table 7 were all estimated using a 2.3 kpc distance. Meanwhile, Trumpler 15 is the oldest, and lowest mass with a less dense core than Trumpler 14. Trumpler 14 and Trumpler 15 are well fitted by King models (King 1962) with a core radius of about 0.7 pc containing about 30–35% of the stars.

Trumpler 16 does not fit into any simple relationship with its two neighbors to the north. It is nearly identical in mass (stellar numbers) to Trumpler 14. The main body of Trumpler 16 and the southeastern extension appear to bracket Trumpler 14 in age and the overall stellar density of the two is nearly the same. The number of high-mass stars traces the total estimated population of all three clusters. Of course, some high mass stars have gone supernova – more in the older clusters. But Trumpler 16 is different. It has no identifiable core and its high mass population is fully distributed. While Ascenso et al. find no mass segregation in Trumpler 14 either, the high mass stars trace the centrally condensed overall population. So overall it would appear that Trumpler 16 is the result of a different mode of star formation.

In this mode the gas within Trumpler 16 appears to have been collected into several lumpy groupings within which the mass clumps were not smoothly distributed. Before a single dynamical timescale, perhaps a triggering event occurred which caused all the clumps to collapse contemporaneously. This is in contrast to the rather organized nature of the other two large clusters. Nonetheless, the mode of star formation which produced Trumpler 16 created a high-mass to low mass star ratio nearly identical to that seen in the other clusters and an XLF nearly identical to that of Trumpler 15, which is well described by a simple King model. This implies that the IMF

and the XLF are robust to different modes of star formation, assuming that the observed IMF and the XLF are not significantly altered by the evolution of cluster members.

## 7. Conclusions

The Chandra ACIS observations of the Trumpler 16 cluster, portions of which were previously studied by Albacete-Colombo et al. (2008), were presented in the framework of the CCCP study. Our analysis shows that Tr 16 is an irregularly shaped cluster. It is not highly centrally condensed but rather breaks up into several sub-clusters. With the benefit of the deep HAWK-I data to identify faint counterparts to the X-ray sources we find no mass segregation in the cluster as a whole. Neither is there apparent mass segregation within the individual sub-clusters. In fact, none of the sub-clusters appear centered on a high mass star with the exception of sub-cluster 14. Other results are summarized as follows:

1. There are 1187 X-ray sources in the total CCCP sample which are classified as likely members of the Trumpler 16 cluster. Positional coincidence matching yields a total of 1047 HAWK-I near-IR counterparts, 1013 of these have three band detections with errors less than 5%.
2. The Trumpler 16 cluster has a roughly circular shape about 11' across (7.4 pc at a distance of 2.3 kpc). Within this outline are seven sub-clusters identified in Paper I. We also discuss a less densely populated, more embedded and younger Southeastern extension to the cluster which is about 10' long running east to west and about 5' north to south (6.7 pc  $\times$  3.4 pc).
3. We confirm the well-established correlations between X-ray flux and near-IR magnitude for high-mass stars and pre-main sequence G and K stars. We also find a weak anti-correlation between X-ray flux and near-IR luminosity for intermediate mass stars.
4. The X-ray luminosity function for stars in Trumpler 16 is compared to the COUP Orion Nebula Cluster XLF. Trumpler 16 shows more low X-ray luminosity and solar mass stars and proportionally fewer high luminosity (intermediate/high mass) stars than in ONC. We estimate the total number of X-ray sources brighter than  $L_{t,c} = 27.5$ , the nominal limit of the COUP, to be about 5 times the number of Class II and Class III sources in the ONC area covered by the COUP survey. This estimate excludes secondary companions.
5. The locations of X-ray detected stars in Trumpler 16 in the near-IR color-magnitude diagram is consistent with a population of 1-3 Myr PMS stars. The extinctions range from near 0 to over 20 in  $A_V$ . There is some spread with 2.0 mag of extinction at  $V$  typically separating the first and fourth quartile.
6. We derive an overall  $K$ -band excess disk frequency of  $8.9 \pm 0.9\%$  using the X-ray selected sample. Excluding the Southeastern extension the disk frequency is about 7%. Both rates

are significantly larger than the rate found in Trumpler 15 – the oldest of the Carina rich clusters – of  $3.8 \pm 0.7\%$  (Wang et al. 2011).

7. We study the seven density enhancements within the main body of the cluster, some of which present unique characteristics. The stellar characteristics of the sub-clusters are very similar. The matrix and the subclusters each contain roughly half the stellar population of Trumpler 16. No mass segregation is seen (i.e., the massive stars are not concentrated in the cluster cores). The pre-main sequence disk fraction found in the subclusters is  $8.4 \pm 1.4\%$  which is consistent with  $6.4 \pm 1.2\%$  found in the surrounding matrix of stars. The exception is the Southeastern extension which has a disk fraction more than a factor of 2 higher. Absorption properties differ, particularly in the Southeastern extension that is heavily extinguished.
8. In addition to the high extinction and higher disk fraction, the Southeastern extension was also found to possess some of the most bolometrically luminous newly identified O star candidates in the region. Taken together, the high disk fraction, high extinction, and luminous O stars are evidence that the Southeastern extension is younger than the core region of Trumpler 16.
9. We detected 29 previously known high mass stars including  $\eta$  Carinae, WR 25, and main sequence stars with spectral types ranging from B2 to O3. Most B0 to B2 stars in this region were not detected. We find marginal evidence that high-mass stars are less absorbed than lower mass stars.
10. The overall structure of Trumpler 16 differs greatly from that of Trumpler 14 and Trumpler 15. Nevertheless the XLF of Trumpler 15 and Trumpler 16 are nearly identical.

We thank the referee for many useful comments. S.J.W. is supported by NASA contract NAS8-03060 (Chandra). This work is supported by Chandra X-ray Observatory grant GO8-9131X (PI: L. Townsley) and by the ACIS Instrument Team contract SV4-74018 (PI: G. Garmire), issued by the Chandra X-ray Center, which is operated by the Smithsonian Astrophysical Observatory for and on behalf of NASA under contract NAS8-03060. AFJM is grateful to NSERC (Canada) and FQRNT (Quebec) for financial aide. The near-infrared observations were collected with the HAWK-I instrument on the VLT at Paranal Observatory, Chile, under ESO program 60.A-9284(K). This research has made use of the SIMBAD database and the VizieR catalogue access tool, operated at CDS, Strasbourg, France.

## REFERENCES

Albacete Colombo, J. F., Méndez, M., & Morrell, N. I. 2003, MNRAS, 346, 704

- Albacete-Colombo, J. F., Damiani, F., Micela, G., Sciortino, S., & Harnden, F. R., Jr. 2008, *A&A*, 490, 1055 (AC08)
- Alexander, D. M., et al. 2003, *AJ*, 126, 539
- Ascenso, J., Alves, J., Vicente, S., Lago, M.T.V.T. 2007 *A&A*, 476, 199
- Brooks, K. J., Garay, G., Nielbock, M., Smith, N., & Cox, P. 2005, *ApJ*, 634, 436
- Broos P. S., et al. 2011a CCCP Catalog paper
- Broos P. S., et al. 2011b CCCP Paper - A Naive Bayes Source Classifier for X-ray Sources
- Broos, P. S., Townsley, L. K., Feigelson, E. D., Getman, K. V., Bauer, F. E., & Garmire, G. P. 2010, *ApJ*, 714, 1582
- Broos, P. S., Feigelson, E. D., Townsley, L. K., Getman, K. V., Wang, J., Garmire, G. P., Jiang, Z., & Tsuboi, Y. 2007, *ApJS*, 169, 353
- Damiani, F., Maggio, A., Micela, G., & Sciortino, S. 1997, *Statistical Challenges in Modern Astronomy II*, 417
- Davidson, K., & Humphreys, R. M. 1997, *ARA&A*, 35, 1
- DeGioia-Eastwood, K., Throop, H., Walker, G., & Cudworth, K. M. 2001, *ApJ*, 549, 578
- Evans, N. R., Seward, F. D., Krauss, M. I., Isobe, T., Nichols, J., Schlegel, E. M., & Wolk, S. J. 2003, *ApJ*, 589, 509
- Feigelson, E. D, et al. 2005, *ApJS*, 160, 379
- Feigelson E. et al. 2011, CCCP Clustering paper (Paper I)
- Feinstein, A., Marraco, H. G., & Muzzio, J. C. 1973, *A&AS*, 12, 331
- Feinstein, A. 1982, *AJ*, 87, 1012
- Forte, J. C. 1978, *AJ*, 83, 1199
- Gagné, M., et al. 2011 CCCP Hot Star paper
- Gaviola, E. 1950, *ApJ*, 111, 408
- Getman, K. V., Feigelson, E. D., Grosso, N., McCaughrean, M. J., Micela, G., Broos, P., Garmire, G., & Townsley, L. 2005, *ApJS*, 160, 353
- Getman, K. V., Feigelson, E. D., Townsley, L., Broos, P., Garmire, G., & Tsujimoto, M. 2006, *ApJS*, 163, 306

- Getman, K. V., Feigelson, E. D., Broos, P. S., Townsley, L. K., & Garmire, G. P. 2010, ApJ, 708, 1760
- Haisch, K. E., Lada, E. A., Lada, C. J. 2001 ApJ, 553, L153
- Herbst, W. 1976, ApJ, 208, 923
- Herschel, J. F. W., Sir 1847, *Results of Observations Made During the Years 1834, 5, 6, 7, 8 at the Cape of Good Hope* (London: Smith, Elder and Co.)
- Kendall, M. 1938,” *Biometrika* 30, 81
- King, I. 1962, AJ, 67, 471
- Levato, H., & Malaroda, S. 1982, PASP, 94, 807
- Morrell, N., Garcia, B., & Levato, H. 1988, PASP, 100, 1431
- Nazé, Y., et al. 2011 CCCP O star paper
- Povich, M. S. et al. 2011 CCCP New OB star paper
- Preibisch, T., & Feigelson, E. D. 2005, ApJS, 160, 390
- Preibisch, T., et al. 2005, ApJS, 160, 401
- Preibisch, T., et al. 2011, CCCP HAWK-I paper
- Sanchawala, K., Chen, W.-P., Lee, H.-T., Chu, Y.-H., Nakajima, Y., Tamura, M., Baba, D., & Sato, S. 2007, ApJ, 656, 462
- Sanchawala, K., et al. 2007, ApJ, 667, 963
- Siess, L., Dufour, E., & Forestini, M. 2000, A&A, 358, 593
- Skiff, B. A. 2010, VizieR Online Data Catalog, 1, 2023
- Skrutskie, M. F., et al. 2006, AJ, 131, 1163
- Smith, N., & Brooks, K. J. 2008, Handbook of Star Forming Regions, Volume II, 138
- Smith, N. 2006, ApJ, 644, 1151
- Smith, N., Gehrz, R. D., Hinz, P. M., Hoffmann, W. F., Hora, J. L., Mamajek, E. E., & Meyer, M. R. 2003, AJ, 125, 1458
- Smith, R. G. 1987, MNRAS, 227, 943
- Spearman, C. 1904, *Amer. J. Psychol.*, 15, 72

- Stelzer, B., Flaccomio, E., Montmerle, T., Micela, G., Sciortino, S., Favata, F., Preibisch, T., & Feigelson, E. D. 2005, *ApJS*, 160, 557
- The, P. S., Bakker, R., & Tjin A Djie, H. R. E. 1980, *A&A*, 89, 209
- Townsley, L., et al. 2011a CCCP Introduction paper
- Townsley, L., et al. 2011b CCCP Diffuse emission paper
- Walborn, N. R. 1971, *ApJ*, 167, L31
- Walborn, N. R. 1973, *ApJ*, 179, 517
- Wang, J., Townsley, L. K., Feigelson, E. D., Broos, P. S., Getman, K. V., Román-Zúñiga, C. G., & Lada, E. 2008, *ApJ*, 675, 464
- Wang, J., Townsley, L. K., Feigelson, E. D., Getman, K. V., Broos, P. S., Garmire, G. P., & Tsujimoto, M. 2007, *ApJS*, 168, 100
- Wolk, S. J., Winston, E., Bourke, T. L., Gutermuth, R., Megeath, S. T., Spitzbart, B. D., & Osten, R. 2010, *ApJ*, 715, 671

Table 1. Basic Properties of Chandra ACIS Point Sources in the Trumpler 16 Region

| Seq. # | Designation<br>CXOGNCJ | R.A.<br>J2000. | Dec.<br>J2000 | Net<br>X-ray Cts | X-ray Cnt<br>err | Class | Sub-<br>cluster |
|--------|------------------------|----------------|---------------|------------------|------------------|-------|-----------------|
| 5277   | 104405.29–594543.4     | 161.022048     | –59.762068    | 24.9             | 5.8              | H2    | Matrix          |
| 5294   | 104405.79–594353.6     | 161.024162     | –59.731567    | 12.4             | 4.7              | H2    | Matrix          |
| 5409   | 104407.86–594315.7     | 161.032779     | –59.721036    | 73.0             | 9.6              | H0    | Matrix          |
| 5416   | 104408.06–594522.4     | 161.033601     | –59.756223    | 36.8             | 6.7              | H2    | Matrix          |
| 5466   | 104409.04–594538.7     | 161.037671     | –59.760751    | 49.5             | 7.4              | H2    | Matrix          |
| 5493   | 104409.75–594338.7     | 161.040642     | –59.727435    | 19.8             | 5.1              | H2    | Matrix          |
| 5496   | 104409.80–594448.0     | 161.040853     | –59.746691    | 49.6             | 7.4              | H2    | Matrix          |
| 5534   | 104410.39–594311.1     | 161.043323     | –59.719771    | 4609.4           | 162.6            | H2    | Matrix          |
| 5541   | 104410.47–594352.7     | 161.043650     | –59.731332    | 15.3             | 4.8              | H2    | Matrix          |
| 5576   | 104411.23–594445.7     | 161.046796     | –59.746034    | 12.6             | 4.0              | H2    | Matrix          |
| 5609   | 104411.89–594414.8     | 161.049575     | –59.737468    | 14.1             | 4.4              | H2    | Matrix          |
| 5629   | 104412.43–594212.6     | 161.051825     | –59.703517    | 18.9             | 4.9              | H2    | Matrix          |
| 5638   | 104412.53–594351.3     | 161.052242     | –59.730934    | 21.9             | 5.2              | H2    | C3              |
| 5647   | 104412.84–594333.1     | 161.053541     | –59.725883    | 16.3             | 4.5              | H2    | C3              |
| 5649   | 104412.86–594344.6     | 161.053617     | –59.729078    | 162.1            | 13.0             | H2    | C3              |

<sup>a</sup>Table 1 with complete notes is published in its entirety in the electronic edition of the *Astrophysical Journal*. A portion is shown here for guidance regarding its form and content.

<sup>b</sup>Column 1: CCCP X-ray catalog sequence number (Broos et al. 2010). Column 2: IAU designation. Columns 3,4: Right ascension and declination for epoch J2000.0 in degrees. Column 5: Net X-ray events detected in the source extraction aperture in the full band (0.5–8 keV; Broos et al. 2011). Column 6: Gaussian error on the net X-ray counts. Column 7: A set of mutually exclusive classification hypotheses defined for each source in Broos et al. (2011) H0 : unclassified; H1: source is a foreground main-sequence star; H2: source is a young star, assumed to be in the Carina complex; H3: source is a Galactic background main-sequence star; H4: source is an extragalactic source. Column 8: The sub-cluster within Trumpler 16. C3, C4, C6 etc (Paper I). ‘Matrix’ means no sub-cluster and not in the Southeastern extension, SEM means no sub-cluster and in the Southeastern extension.

Table 2. XPHOT Derived Properties of Chandra ACIS Point Sources in the Trumpler 16 Region

| Seq. # | Designation        | Median<br>energy [keV] | error<br>Med. energy | Log flux<br>[ergs cm <sup>2</sup> sec <sup>-1</sup> ] | Statistical err<br>log flux | Systematic err<br>log flux | Log $N_{\text{H}}$<br>[cm <sup>-2</sup> ] | Statistical err<br>Log $N_{\text{H}}$ | Systematic err<br>Log $N_{\text{H}}$ |
|--------|--------------------|------------------------|----------------------|---|-----------------------------|----------------------------|---|---------------------------------------|--------------------------------------|
| 5277   | 104405.29–594543.4 | 0.97                   | 0.12                 | -14.64  | -15.19                      | -16.33                     | 20.26                                     | 0.00                                  | 0.26                                 |
| 5294   | 104405.79–594353.6 | 1.08                   | 0.19                 | -14.87  | -15.21                      | -16.56                     | 20.26                                     | 0.36                                  | 0.26                                 |
| 5409   | 104407.86–594315.7 | 2.84                   | 0.24                 | -13.23  | -13.98                      | -13.97                     | 22.41                                     | 0.09                                  | 0.05                                 |
| 5416   | 104408.06–594522.4 | 1.76                   | 0.16                 | -13.95  | -14.56                      | -14.50                     | 21.95                                     | 0.15                                  | 0.09                                 |
| 5466   | 104409.04–594538.7 | 1.61                   | 0.14                 | -13.90  | -14.55                      | -14.46                     | 21.78                                     | 0.18                                  | 0.12                                 |
| 5493   | 104409.75–594338.7 | 1.26                   | 0.15                 | -14.35  | -14.78                      | -14.72                     | 20.98                                     | 0.61                                  | 0.50                                 |
| 5496   | 104409.80–594448.0 | 1.48                   | 0.13                 | -13.97  | -14.60                      | -14.68                     | 21.60                                     | 0.24                                  | 0.12                                 |
| 5534   | 104410.39–594311.1 | 1.51                   | 0.03                 | -11.24  | -12.63                      | -12.21                     | 21.48                                     | 0.06                                  | 0.12                                 |
| 5541   | 104410.47–594352.7 | 1.88                   | 0.28                 | -14.17  | -14.56                      | -14.71                     | 22.08                                     | 0.21                                  | 0.08                                 |
| 5576   | 104411.23–594445.7 | 1.35                   | 0.24                 | -14.65  | -14.91                      | -15.00                     | 21.48                                     | 0.85                                  | 0.22                                 |
| 5607   | 104411.88–594223.2 | 1.47                   | 0.28                 | -14.60  | -14.87                      | -14.89                     | 21.60                                     | 0.68                                  | 0.24                                 |
| 5609   | 104411.89–594414.8 | 1.93                   | 0.44                 | -14.23  | -14.54                      | -14.48                     | 22.15                                     | 0.31                                  | 0.11                                 |
| 5629   | 104412.43–594212.6 | 1.99                   | 0.31                 | -14.10  | -14.54                      | -14.58                     | 22.15                                     | 0.21                                  | 0.08                                 |
| 5638   | 104412.53–594351.3 | 1.29                   | 0.16                 | -14.46  | -14.90                      | -14.85                     | 21.30                                     | 0.67                                  | 0.35                                 |
| 5647   | 104412.84–594333.1 | 1.42                   | 0.18                 | -14.20  | -14.58                      | -14.60                     | 21.60                                     | 0.43                                  | 0.18                                 |
| 5649   | 104412.86–594344.6 | 2.02                   | 0.12                 | -13.18  | -14.11                      | -13.80                     | 22.11                                     | 0.07                                  | 0.09                                 |

<sup>a</sup>Table 2 with complete notes is published in its entirety in the electronic edition of the Astrophysical Journal. A portion is shown here for guidance regarding its form and content.

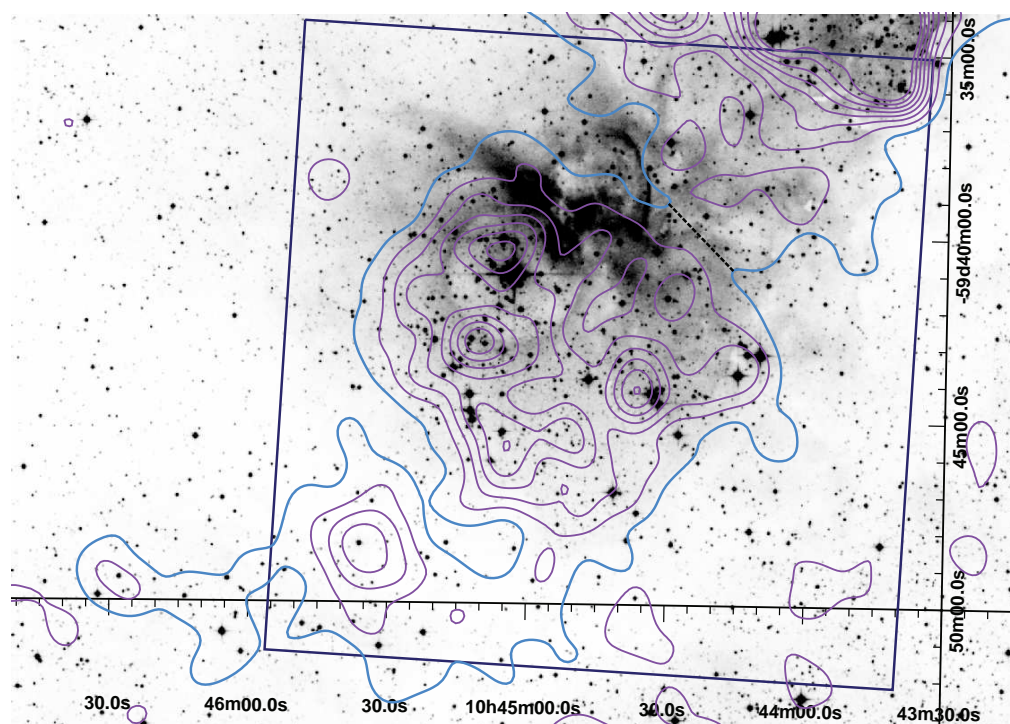


Fig. 1.— Trumpler 16 cluster overview. The background image is a far-red image from the Digitized Sky Survey (DSS2-I; squared scaling). The square indicates the field of view of ObsID 6204. The contours indicate an increase of source density of 1 X-ray source per  $30''$ . The outer thick contour indicates the extent of the Trumpler 14 and 16 clusters.  $\eta$  Car is the bright star near the north-east X-ray source concentration. The dashed line indicates our boundary between Trumpler 16 and Trumpler 14 (to the Northwest).

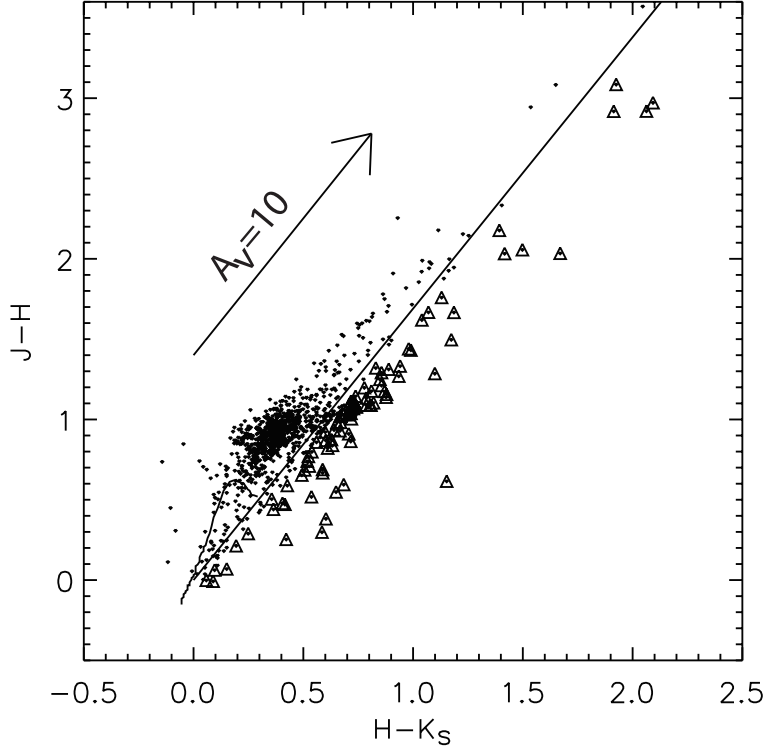


Fig. 2.— Near-infrared color-color diagram of 1013 CCCP sources in Trumpler 16 (including the Southeastern extension) using the HAWK-I data (Preibisch et al. 2011). A reddening vector of 10 visual magnitudes is indicated. The short curve in the lower-left indicates the nominal main sequence. The parallel lines indicate the reddening band for stars without optically thick disks in the  $K_S$  band. Triangles indicate stars at least 0.1 magnitudes to the right of the reddening band; these are probable disk systems with optically thick disks in the  $K_S$  band. We find 9% of the X-ray sources which are associated with probable cluster members have disks. Several of these are high mass stars. Similar analysis was carried out separately on each subcluster within Trumpler 16.

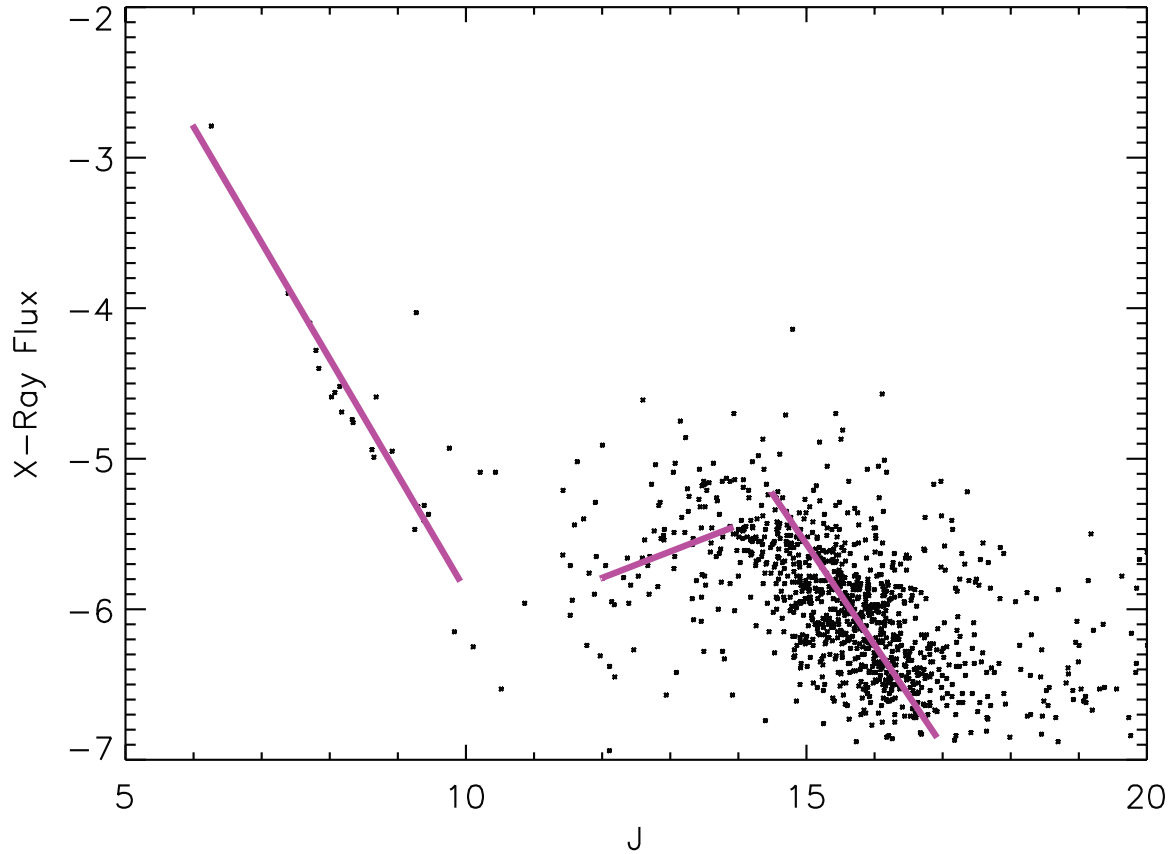


Fig. 3.— The X-ray flux (in units of  $\log \text{photons sec}^{-1}\text{cm}^{-2}$ ) compared to the J band magnitude. X-ray sources with  $J < 11$  (O and early-B stars) and within  $14 < J < 17$  (pre-main sequence stars) show well-known correlations between X-ray and optical luminosities. The weak anti-correlation at intermediate luminosities ( $12 < J < 14$ ) is newly reported here.

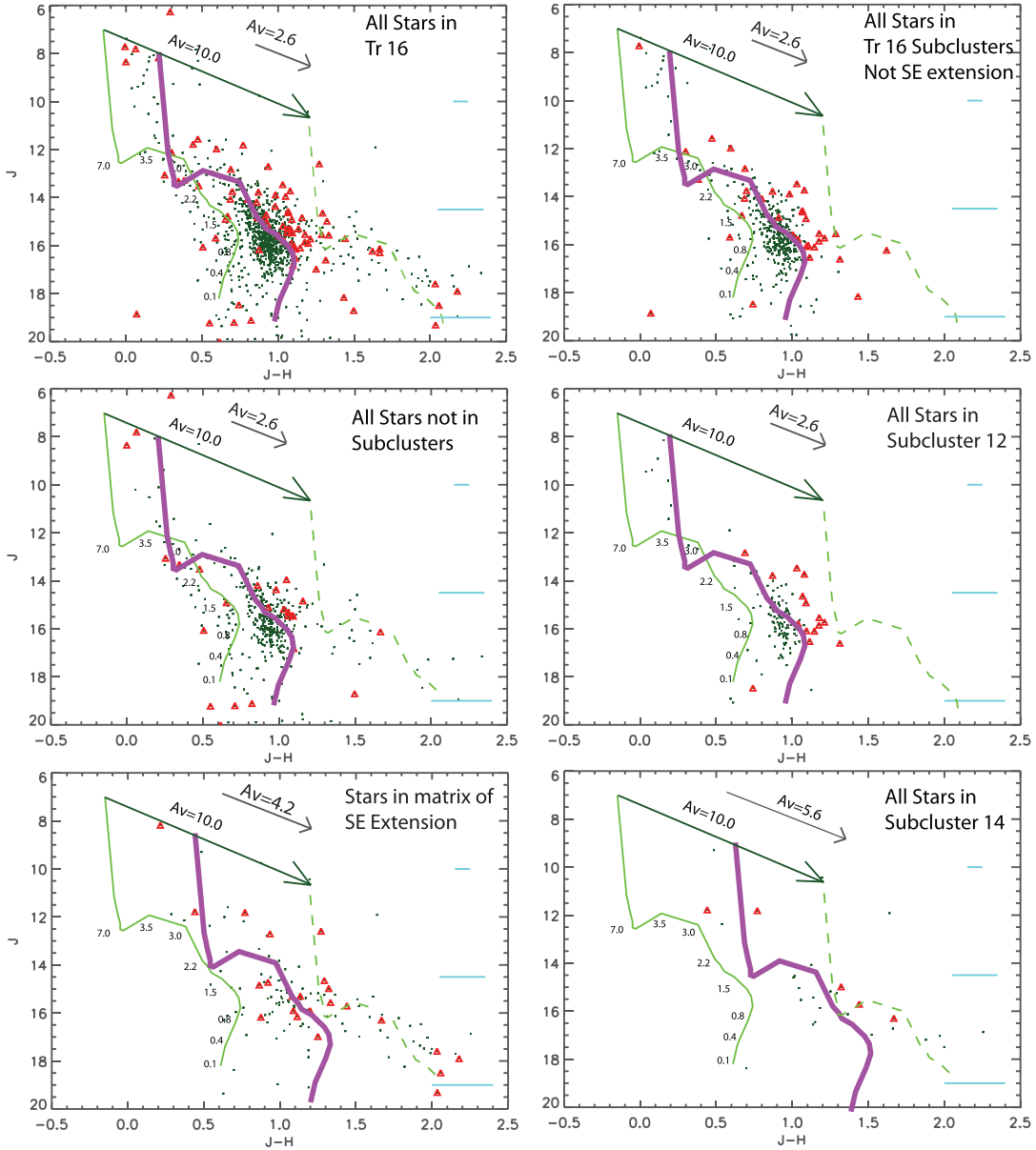


Fig. 4.— Near-infrared color-magnitude diagrams for Trumpler 16 and several of its sub-structures. The green solid line indicates a 3 Myr isochrone derived from Siess et al. (2000) set at a distance modulus of 11.8. The dashed green line is the same isochrone with 10  $A_V$  of extinction applied. The thick purple line is an approximate fit of the isochrone to the data with only the extinction being allowed as a free parameter. The short arrow in the upper middle of each frame shows the derived extinction for each region. The triangles indicate stars with disks as derived from the IR-color-color diagram. All of the regions in the main part of Trumpler 16 fit well to an extinction of  $A_V = 3.3$ . The stars in the Southeastern extension average about 150% this extinction, and its Sub-cluster 14 is even more absorbed. The bulk of the disked stars are more absorbed than the cluster mean. The cyan horizontal lines indicate rough color error bars.

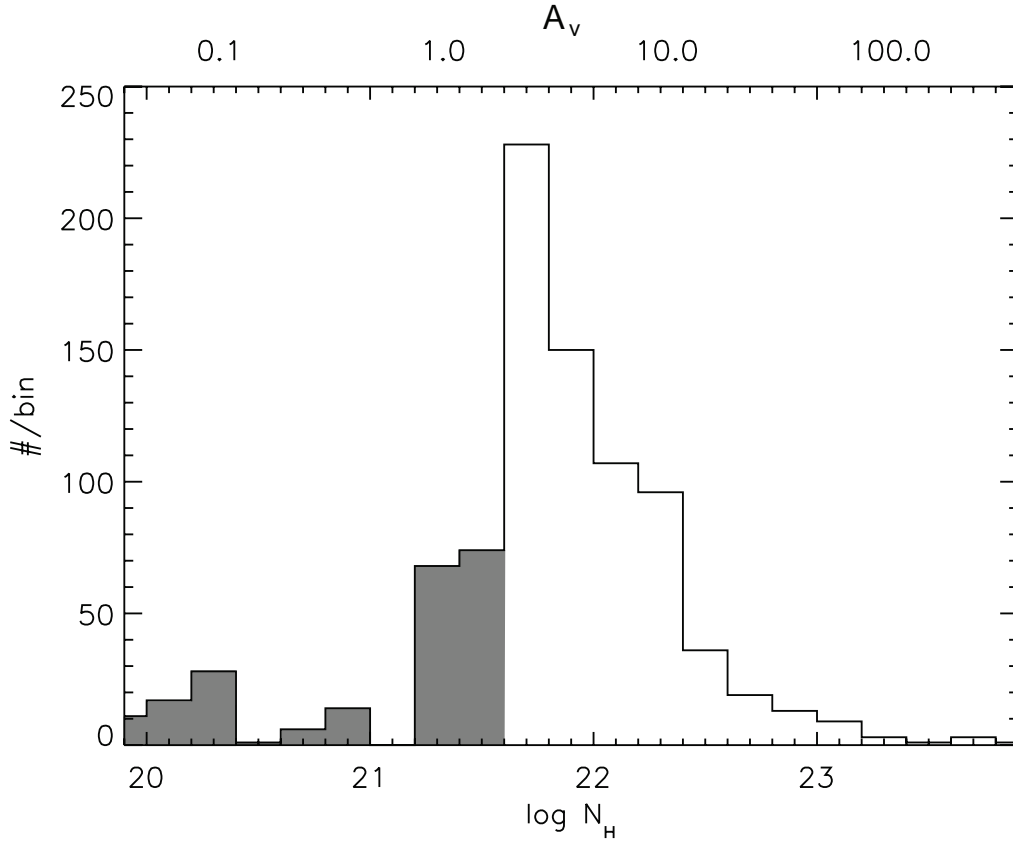


Fig. 5.— Histogram of  $\log N_{\text{H}}$  of 687 X-ray sources in Trumpler 16 as measured using the XPHOT method. The top axis gives the approximate optical extinction ( $A_V$ ) using a conversion ratio of  $N_{\text{H}}/A_V = 1.6 \times 10^{21}$  (Vuong et al. 2003). The histogram is in grey below  $\log N_{\text{H}} = 21.6$  to indicate the less robust nature of these measurements (see text).

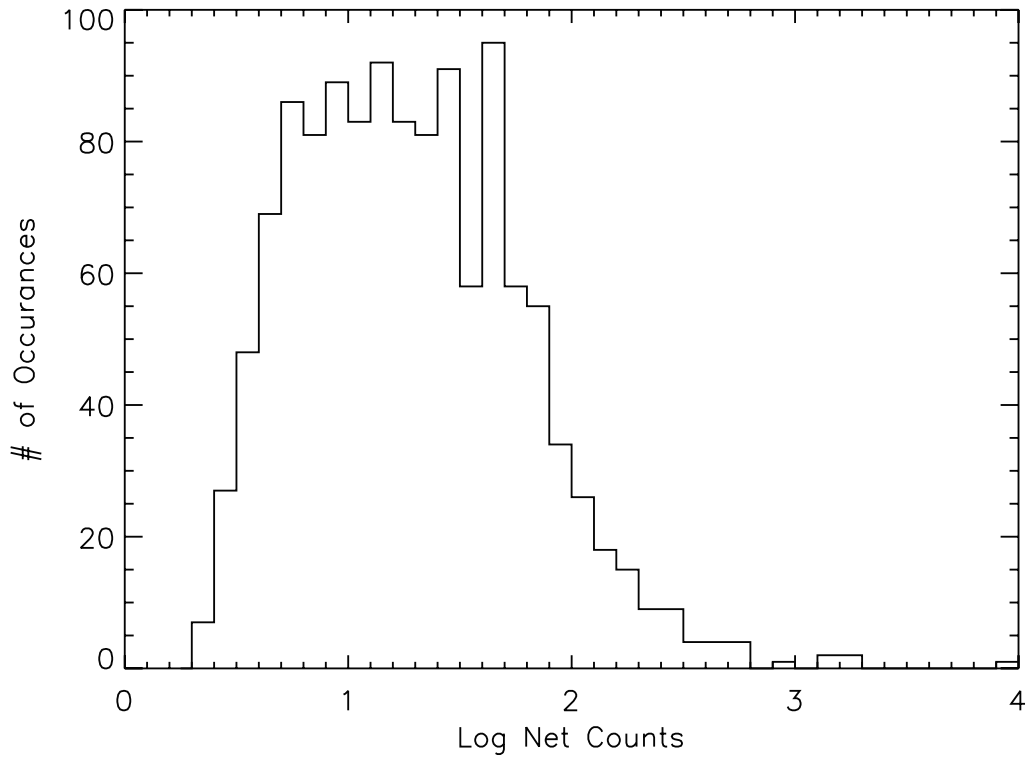


Fig. 6.— Histogram distribution of the net counts from the 1232 X-rays sources detected in the Trumpler 16 region.

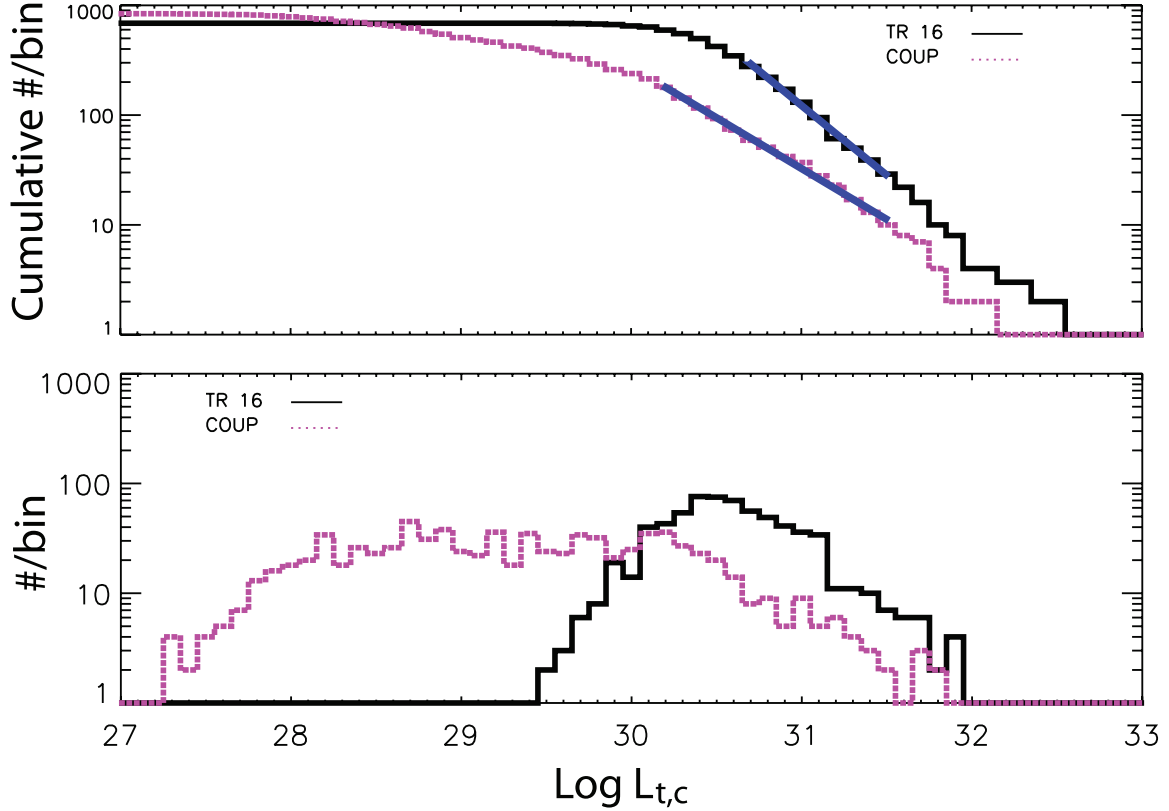


Fig. 7.— Top: Power-law fits to the Trumpler 16 data from  $\log L_{t,c} = 30.7\text{--}31.5$  and to the COUP data from  $\log L_{t,c} = 30.2\text{--}31.5$  are shown by blue line. The Trumpler 16 distribution has a slope of  $\Gamma = -1.27$ , while the COUP data have a slope of  $\Gamma = -0.92$ . Bottom: Histogram of absorption-corrected, total-band (0.5–8keV) X-ray luminosities of all 687 X-ray sources in Trumpler 16 (black, solid) for which XPHOT could calculate luminosities and which are not in the SE extension. These are compared to the COUP sample (magenta, dotted) of 839 sources from the ONC.

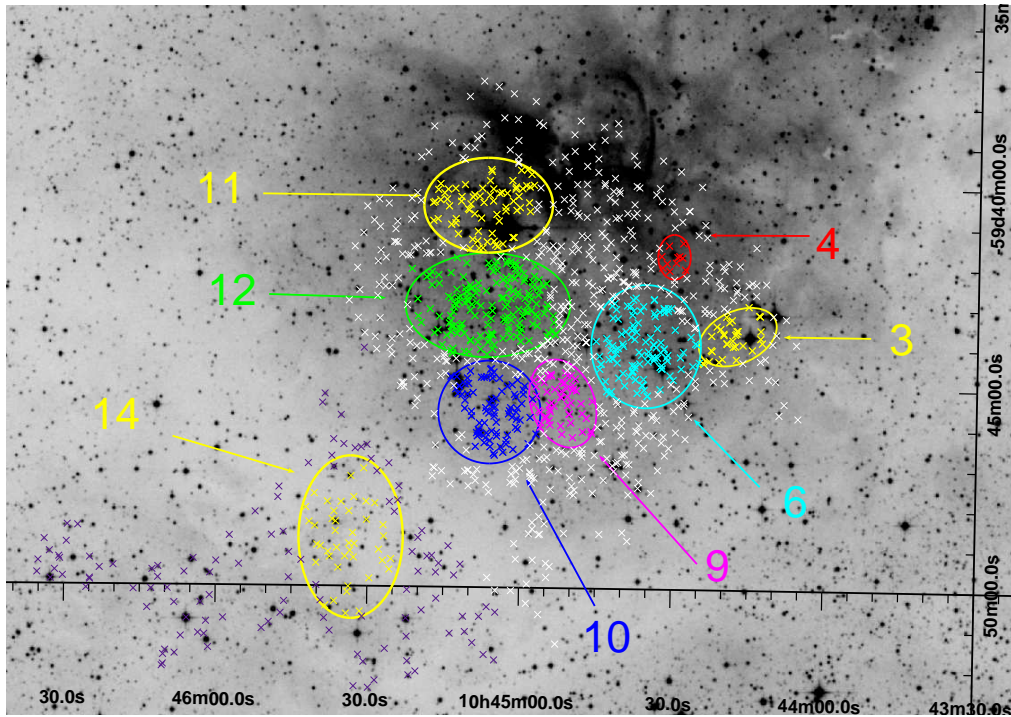


Fig. 8.— The sub-clusters within Trumpler 16 with X-ray sources noted by  $\times$  symbols. Each sub-cluster is labeled with designations from Paper I and shown by an approximate ellipse. In the color version the various sub-clusters are indicated by color as well. Members of the matrix are indicated in white and occasionally cross into region ovals as the latter are approximated. The background image is the same as Fig. 1, but linearly scaled.

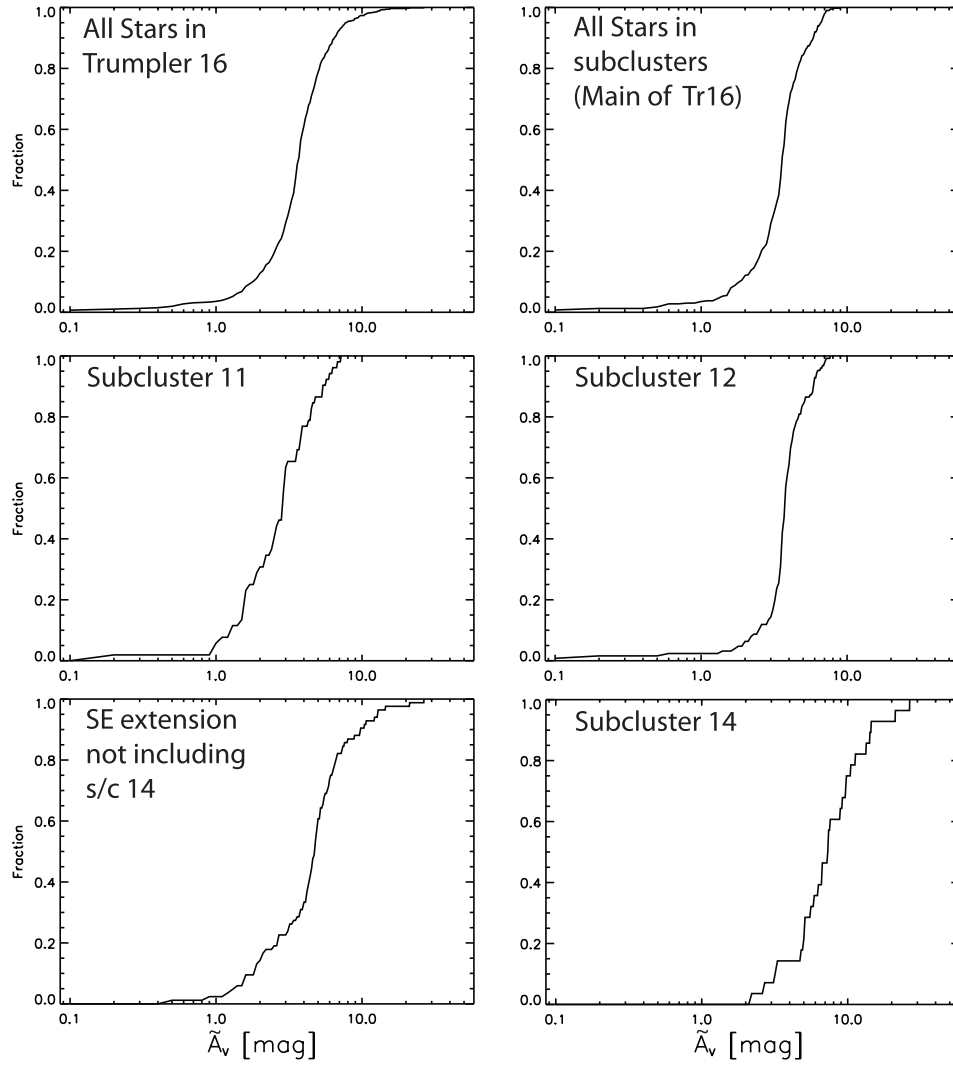


Fig. 9.— The extinction functions for several regions within Trumpler 16.

Table 3. Summary of Metric for Each Sub-cluster

| Sub-cluster | No. Sources | Density<br>[src pc <sup>-2</sup> ] | Disk Fraction | $\langle \tilde{A}_V \rangle$<br>25/50/75<br>percentiles | Abs. $K_S$<br>25/50/75<br>percentiles |
|-------------|-------------|------------------------------------|---------------|--|---------------------------------------|
| All         | 1187        | 27                                 | 8.9±0.9%      | 2.9/3.7/4.8  | 1.25/2.0/2.5                          |
| no sub      | 506         | ...                                | 6.4±1.2%      | 2.8/3.8/5.2  | 1.0/2.0/2.5                           |
| all N. sub  | 525         | ...                                | 8.4±1.4%      | 2.9/3.6/4.3  | 1.25/2.0/2.5                          |
| 3           | 33          | 33                                 | 14.8±7.4%     | 3.0/3.8/4.5  | 1.75/2.0/2.25                         |
| 4           | 11          | 34                                 | 25.0±17.7%    | 2.7/3.5/3.8  | 1.5/2.5/2.5                           |
| 6           | 109         | 45                                 | 6.8±2.8%      | 2.9/3.6/4.1  | 1.25/2.25/2.75                        |
| 9           | 53          | 48                                 | 4.4±3.1%      | 2.8/3.7/4.3  | 1.75/2.25/3.25                        |
| 10          | 82          | 42                                 | 5.4±2.7%      | 3.1/3.7/4.5  | 1.0/2.0/2.5                           |
| 11          | 71          | 27                                 | 7.0±3.5%      | 1.9/2.9/3.9  | 1.25/1.75/2.5                         |
| 12          | 166         | 42                                 | 10.6±2.7%     | 3.4/3.8/4.3  | 1.25/2.0/2.5                          |
| SE ext      | 116         | ...                                | 17.8±4.2%     | 3.2/4.8/6.3  | 0.5/1.5/2.5                           |
| 14          | 40          | 10                                 | 21.2±8.0%     | 5.1/7.4/10.5   | 0.25/0.75/1.5                         |
| SE all      | 156         | 9                                  | 18.7±3.7%     | 4.3/5.6/8.6  | 0.5/1.25/2.25                         |

Table 4. CCCP Detected OB Stars in the Trumpler 16 Region <sup>1</sup>

| Seq. # | sub Cl. | R.A.<br>(J2000.) | Dec.<br>(J2000.) | Name                   | SpType               | V<br>(mag) | X-ray Cts<br>(0.5-8.0 keV) |
|--------|---------|------------------|------------------|------------------------|----------------------|------------|----------------------------|
| 5294   | Matrix  | 10 44 05.82      | −59 35 11.7      | Cl* Trumpler 16 MJ 224 | B1V                  | 11.14      | 12.4                       |
| 5534   | Matrix  | 10 44 10.39      | −59 43 11.1      | WR 25                  | WN6h + OB?           | 8.1        | 24609                      |
| 5665   | C3      | 10 44 13.20      | −59 43 10.2      | Cl* Trumpler 16 MJ 257 | O3/4If               | 10.8       | 359.2                      |
| 6676   | C6      | 10 44 32.34      | −59 44 31.0      | HD 93204               | O5.5V((f))           | 8.42       | 310.8                      |
| 6773   | C6      | 10 44 33.74      | −59 44 15.5      | HD 93205               | O3.5V((f+)) + O8V    | 7.75       | 1408.7                     |
| 6955   | Matrix  | 10 44 36.70      | −59 47 29.7      | Cl* Trumpler 16 MJ 359 | O8V                  | 10.89      | 68.9                       |
| 6691   | Matrix  | 10 44 37.17      | −59 40 01.3      | Cl* Trumpler 16 MJ 357 | B0.5V                | 11.57      | 6.1                        |
| 7224   | Matrix  | 10 44 40.99      | −59 40 10.2      | Cl* Trumpler 16 MJ 372 | B0V                  | 11.4       | 14.2                       |
| 7277   | Matrix  | 10 44 41.80      | −59 46 56.4      | Cl Trumpler 16 100     | O5.5V                | 8.6        | 976                        |
| 7621   | Matrix  | 10 44 47.31      | −59 43 53.2      | CD−59 3303             | O7V + O9.5V + B0.2IV | 8.8        | 108.4                      |
| 8036   | Matrix  | 10 44 54.06      | −59 41 29.4      | Cl* Trumpler 16 MJ 427 | B1V                  | 10.9       | 173.1                      |
| 8380   | C12     | 10 44 59.90      | −59 43 14.8      | Cl Trumpler 16 26      | B1.5V                | 11.66      | 9.5                        |
| 8579   | C11     | 10 45 03.16      | −59 40 12.5      | Cl* Trumpler 16 MJ 467 | B0.5V                | 10.82      | 6.6                        |
| ...    | ...     | 10 45 03.55      | −59 41 04.0      | $\eta$ Carinæ          | pec.                 | 6          |                            |
| 8648   | C11     | 10 45 04.78      | −59 40 53.5      | Cl Trumpler 16 64      | B1.5V:b              | 10.7       | 281.2                      |
| 8705   | C10     | 10 45 05.80      | −59 45 19.6      | Cl* Trumpler 16 MJ 484 | O7V                  | 10         | 204.9                      |
| 8707   | C12     | 10 45 05.83      | −59 43 07.7      | Cl* Trumpler 16 MJ 481 | O9.5V                | 9.77       | 102.2                      |
| 8714   | C11     | 10 45 05.92      | −59 40 05.9      | HD 303308              | O4V((f))             | 8.17       | 1654                       |
| 8758   | C12     | 10 45 06.72      | −59 41 56.6      | Cl* Trumpler 16 MJ 488 | O8.5V                | 9.9        | 91.8                       |
| 8831   | C11     | 10 45 08.23      | −59 40 49.4      | CPD−59 2628            | O9.5V + B0.3V        | 9.5        | 65.5                       |
| 8832   | C10     | 10 45 08.24      | −59 46 07.0      | Cl* Trumpler 16 MJ 496 | O8.5V                | 10.93      | 1909.4                     |
| 9028   | C10     | 10 45 12.22      | −59 45 00.4      | HD 93343               | O7V(n)               | 9.7        | 204.9                      |
| 9038   | C12     | 10 45 12.65      | −59 42 48.7      | Cl* Trumpler 16 MJ 513 | B2:V                 | 11.2       | 14.9                       |
| 9044   | C10     | 10 45 12.72      | −59 44 46.2      | CPD−59 2635            | O8.5                 | 9.3        | 384.1                      |
| 9050   | Matrix  | 10 45 12.87      | −59 44 19.3      | CPD−59 2636            | O8.5                 | 9.3        | 579.7                      |
| 9195   | C12     | 10 45 16.52      | −59 43 37.0      | Cl Trumpler 16 112     | O4.5((f))            | 9.3        | 624.4                      |
| 9344   | C12     | 10 45 20.57      | −59 42 51.2      | Cl* Trumpler 16 MJ 554 | O8.5V                | 10.09      | 77.1                       |
| 9857   | C14     | 10 45 36.32      | −59 48 23.2      | Cl* Trumpler 16 MJ 596 | O5.5Vz + O9.5V       | 12.1       | 69                         |
| 10748  | Matrix  | 10 46 05.70      | −59 50 49.4      | LS 1886                | O4V                  | 10.7       | 544.6                      |

<sup>1</sup>Adapted from Skiff (2010)

Table 5. IR colors of CCCP Detected OB Stars in the Trumpler 16 Region<sup>1</sup>

| Seq. # | Name                   | J      | Jerr  | H      | Herr  | K      | Kerr  | $A_V(J - K)$ | $A_V(J - H)$ |
|--------|------------------------|--------|-------|--------|-------|--------|-------|--------------|--------------|
| 5294   | Cl* Trumpler 16 MJ 224 | 15.459 | 0.002 | 14.398 | 0.001 | 13.712 | 0.001 | 8.88         | 8.69         |
| 5534   | WR 25                  | 6.26   | 0.007 | 5.97   | 0.023 | 5.721  | 0.015 | 3.37         | 3.16         |
| 5665   | Cl* Trumpler 16 MJ 257 | 7.84   | 0.013 | 7.381  | 0.037 | 7.061  | 0.017 | 4.46         | 4.37         |
| 6676   | HD 93204               | 8.026  | 0.021 | 7.987  | 0.035 | 7.97   | 0.029 | 1.17         | 1.36         |
| 6773   | HD 93205               | 7.389  | 0.009 | 7.386  | 0.027 | 7.342  | 0.029 | 1.13         | 1.10         |
| 6955   | Cl* Trumpler 16 MJ 359 | 9.384  | 0.017 | 9.142  | 0.019 | 9.007  | 0.018 | 2.63         | 2.81         |
| 6691   | Cl* Trumpler 16 MJ 357 | ...    | ...   | ...    | ...   | ...    | ...   | ...          | ...          |
| 7224   | Cl* Trumpler 16 MJ 372 | 10.106 | 0.021 | 9.898  | 0.019 | 9.866  | 0.02  | 2.01         | 2.57         |
| 7277   | Cl Trumpler 16 100     | 7.798  | 0.015 | 7.735  | 0.035 | 7.639  | 0.025 | 1.64         | 1.53         |
| 7621   | CD–59 3303             | 8.343  | 0.013 | 8.344  | 0.021 | 8.286  | 0.019 | 1.17         | 1.07         |
| 8036   | Cl* Trumpler 16 MJ 427 | 10.209 | 0.047 | 10.153 | 0.069 | 10.16  | 0.039 | 1.14         | 1.48         |
| 8380   | Cl Trumpler 16 26      | 10.863 | 0.017 | 10.66  | 0.025 | 10.509 | 0.021 | 2.53         | 2.53         |
| 8579   | Cl* Trumpler 16 MJ 467 | ...    | ...   | ...    | ...   | ...    | ...   | ...          | ...          |
| ...    | $\eta$ Carinae         | ...    | ...   | ...    | ...   | ...    | ...   | ...          | ...          |
| 8648   | Cl Trumpler 16 64      | ...    | ...   | ...    | ...   | ...    | ...   | ...          | ...          |
| 8705   | Cl* Trumpler 16 MJ 484 | 8.649  | 0.019 | 8.416  | 0.017 | 8.335  | 0.021 | 2.34         | 2.75         |
| 8707   | Cl* Trumpler 16 MJ 481 | 8.916  | 0.007 | 8.8    | 0.021 | 8.762  | 0.02  | 1.61         | 1.91         |
| 8714   | HD 303308              | 7.707  | 0.013 | 7.714  | 0.033 | 7.625  | 0.045 | 1.29         | 1.03         |
| 8758   | Cl* Trumpler 16 MJ 488 | 9.45   | 0.015 | 9.412  | 0.031 | 9.36   | 0.027 | 1.32         | 1.35         |
| 8831   | CPD–59 2628            | 9.249  | 0.019 | 9.136  | 0.017 | 9.253  | 0.061 | 0.89         | 1.89         |
| 8832   | Cl* Trumpler 16 MJ 496 | 9.27   | 0.017 | 8.96   | 0.021 | 8.813  | 0.019 | 3.00         | 3.30         |
| 9028   | HD 93343               | 8.681  | 0.009 | 8.543  | 0.019 | 8.434  | 0.019 | 2.04         | 2.07         |
| 9038   | Cl* Trumpler 16 MJ 513 | 9.83   | 0.019 | 9.646  | 0.025 | 9.531  | 0.023 | 2.28         | 2.40         |
| 9044   | CPD–59 2635            | 8.33   | 0.011 | 8.18   | 0.033 | 8.091  | 0.017 | 2.00         | 2.15         |
| 9050   | CPD–59 2636            | 8.076  | 0.017 | 7.894  | 0.031 | 7.756  | 0.017 | 2.37         | 2.38         |
| 9195   | Cl Trumpler 16 112     | 8.147  | 0.005 | 7.993  | 0.021 | 7.884  | 0.033 | 2.11         | 2.18         |
| 9344   | Cl* Trumpler 16 MJ 554 | 9.387  | 0.017 | 9.309  | 0.021 | 9.257  | 0.018 | 1.50         | 1.64         |
| 9857   | Cl* Trumpler 16 MJ 596 | 9.293  | 0.021 | 8.809  | 0.027 | 8.505  | 0.023 | 4.51         | 4.55         |
| 10748  | LS 1886                | 8.176  | 0.013 | 7.962  | 0.035 | 7.768  | 0.025 | 2.77         | 2.61         |

<sup>1</sup>Adapted from Skiff (2010)

Table 6. High Mass Stars in the Trumpler 16 Region - Not Detected in X-rays<sup>1</sup>

| R.A.<br>(J2000.) | Dec.<br>(J2000.) | Name                   | SpType | V<br>(mag) | sub Cl. |
|------------------|------------------|------------------------|--------|------------|---------|
| 10 44 13.80      | −59 42 57.0      | Cl* Trumpler 16 MJ 261 | B0V    | 12.1       | Matrix  |
| 10 44 14.75      | −59 42 51.7      | Cl* Trumpler 16 MJ 263 | B0.5V  | 11.9       | Matrix  |
| 10 44 26.48      | −59 41 02.7      | Cl* Trumpler 16 MJ 306 | B1.5V  | 9.88       | Matrix  |
| 10 44 28.98      | −59 42 34.2      | Cl* Trumpler 16 MJ 323 | B2V    | 12.1       | Matrix  |
| 10 44 30.49      | −59 41 40.5      | Cl* Trumpler 16 MJ 329 | B1V    | 10.88      | C4      |
| 10 44 32.89      | −59 40 25.9      | Cl* Trumpler 16 MJ 339 | B1V    | 10.8       | Matrix  |
| 10 44 38.66      | −59 48 14.2      | Cl Trumpler 16 20      | B1:V   | 10.2       | Matrix  |
| 10 44 40.32      | −59 41 48.8      | Cl* Trumpler 16 MJ 370 | B1V    | 10.77      | Matrix  |
| 10 44 58.79      | −59 49 21.1      | Hen 3–480              | em     | 11.5       | Matrix  |
| 10 45 00.24      | −59 43 34.4      | Cl Trumpler 16 25      | B2V    | 11.88      | C12     |
| 10 45 02.19      | −59 42 01.1      | Cl* Trumpler 16 MJ 466 | B1V    | 10.96      | C12     |
| 10 45 05.18      | −59 41 42.4      | Cl* Trumpler 16 MJ 477 | B1V    | 12.1       | C12/11  |
| 10 45 05.88      | −59 44 18.9      | Cl* Trumpler 16 MJ 483 | B2V    | 11.5       | C12     |
| 10 45 09.65      | −59 40 08.5      | Cl* Trumpler 16 MJ 499 | B2V    | 12.2       | C11     |
| 10 45 09.74      | −59 42 57.1      | Cl* Trumpler 16 MJ 501 | B1V    | 11.69      | C12     |
| 10 45 11.18      | −59 41 11.2      | Cl* Trumpler 16 MJ 506 | B1V    | 10.78      | C11     |
| 10 45 19.42      | −59 39 37.3      | Cl* Trumpler 16 MJ 547 | B1.5V  | 12.2       | Matrix  |
| 10 45 31.86      | −59 51 09.4      | BM VII 10              | S      | 13.6       | SEM     |
| 10 45 44.61      | −59 50 41.1      | FO 16                  | OB-    | 12.34      | SEM     |
| 10 45 54.80      | −59 48 15.4      | Trumpler 16 MJ 633     | em     | 13.1       | SEM     |
| 10 46 32.62      | −59 49 50.0      | HD 93538               | A5/8   | 9.6        | SEM     |

<sup>1</sup>Adapted from Skiff (2010)

Table 7. Comparison of the Three Massive Clusters in the Carina Nebula

|   | Trumpler 14 <sup>1</sup> | Trumpler 15 <sup>2</sup> | Trumpler 16                   |
|---|--------------------------|--------------------------|-------------------------------|
| X-Ray Sources:                            |                          |                          |                               |
| Probable Members <sup>3</sup> :           | 1378                     | 829                      | 1187                          |
| HAWK-I Detections <sup>4</sup> :          | 1219                     | 748                      | 1050                          |
| XLF ( $\Gamma$ )                          | ...                      | $\sim -1.27$             | $\sim -1.27$                  |
| Estimated # Stars ( $\pm 10\%$ )          | 12,500 <sup>5</sup>      | 5,900                    | 14,000                        |
| High Mass Stars <sup>6</sup>              | 46                       | 24                       | 57                            |
| Area [ pc <sup>2</sup> ]                  |                          |                          |                               |
| Core:                                     | 1.4                      | 1.4                      | ...                           |
| Total:                                    | 95                       | 50                       | 80                            |
| Density [X-ray sources pc <sup>-2</sup> ] |                          |                          |                               |
| Core:                                     | 300                      | 200                      | ...                           |
| Total:                                    | 14.5                     | 16.6                     | 14.8                          |
| Disk Fraction [%]                         | 9.7 <sup>4</sup>         | 3.8                      | 7.4 – north<br>17.8 – SE ext. |
| Age                                       | 2-3 Myr <sup>4</sup>     | 5-10 Myr                 | 3-4 Myr <sup>4</sup>          |

<sup>1</sup>Reference: Acenoso et al. (2008) unless otherwise noted.

<sup>2</sup>Reference: Wang et al. (2011) unless otherwise noted.

<sup>3</sup>Reference: Broos et al. (2011)

<sup>4</sup>Reference: Preibisch et al. (2011)

<sup>5</sup>See text for this calculation.

<sup>6</sup>Reference: Skiff et al. (2010)